

# Presynaptic NMDARs in the Hippocampus Facilitate Transmitter Release at Theta Frequency

Lindsay McGuinness,<sup>1</sup> Chanel Taylor,<sup>1</sup> Ruth D.T. Taylor,<sup>1</sup> Christopher Yau,<sup>2</sup> Tobias Langenhan,<sup>1</sup> Michael L. Hart,<sup>1</sup> Helen Christian,<sup>3</sup> Patricia W. Tynan,<sup>1</sup> Peter Donnelly,<sup>2</sup> and Nigel J. Emptage<sup>1,\*</sup>

<sup>1</sup>Department of Pharmacology, University of Oxford, Mansfield Road, Oxford OX1 3QT, UK

<sup>2</sup>Henry Wellcome Centre for Gene Function, University of Oxford, South Parks Road, Oxford OX1 3TG, UK

<sup>3</sup>Department of Physiology, Anatomy and Genetics, University of Oxford, South Parks Road, Oxford OX1 3QX, UK

\*Correspondence: nigel.emptage@pharm.ox.ac.uk

DOI 10.1016/j.neuron.2010.11.023

## SUMMARY

A rise in  $[Ca^{2+}]_i$  provides the trigger for neurotransmitter release at neuronal boutons. We have used confocal microscopy and  $Ca^{2+}$  sensitive dyes to directly measure the action potential-evoked  $[Ca^{2+}]_i$  in the boutons of Schaffer collaterals. This reveals that the trial-by-trial amplitude of the evoked  $Ca^{2+}$  transient is bimodally distributed. We demonstrate that “large”  $Ca^{2+}$  transients occur when presynaptic NMDA receptors are activated following transmitter release. Presynaptic NMDA receptor activation proves critical in producing facilitation of transmission at theta frequencies. Because large  $Ca^{2+}$  transients “report” transmitter release, their frequency on a trial-by-trial basis can be used to estimate the probability of release,  $p_r$ . We use this novel estimator to show that  $p_r$  increases following the induction of long-term potentiation.

## INTRODUCTION

In central neurones, action potential (AP)-induced depolarization of the plasma membrane results in a transient rise in intracellular  $Ca^{2+}$  concentration,  $[Ca^{2+}]_i$ . The rise activates the fusion of presynaptic vesicles and the release of neurotransmitter (Katz and Miledi, 1970; Mulkey and Zucker, 1991; Neher, 1998). The increase in  $[Ca^{2+}]_i$  primarily arises from an influx of  $Ca^{2+}$  via voltage-dependent  $Ca^{2+}$  channels, VDCCs (Augustine, 2001; Koester and Sakmann, 2000), although it is clear that  $Ca^{2+}$  influx triggers further  $Ca^{2+}$  release, such as release of  $Ca^{2+}$  from intracellular stores (Emptage et al., 2001; Llano et al., 2000; Simkus and Stricker, 2002; Verstreken et al., 2005). Interestingly, within the central nervous system (CNS), the AP-evoked  $[Ca^{2+}]_i$  rise exhibits large differences, both between boutons along a single axon collateral (Koester and Sakmann, 2000; Llano et al., 1997) and within individual boutons on a trial-by-trial basis (Frenguelli and Malinow, 1996; Kirischuk and Grantyn, 2002; Llano et al., 1997; Mackenzie et al., 1996; Wu and Saggau, 1994b). Given the steep power relationship between  $Ca^{2+}$  influx and exocytosis (Dodge and Rahamimoff, 1967), these variations in  $[Ca^{2+}]_i$  are likely to have a dramatic influence on neurotransmitter release

(Borst and Sakmann, 1996; Kirischuk and Grantyn, 2002; Wu and Saggau, 1994a, b). Although it is easy to envisage that differences in  $Ca^{2+}$  channel type or density within a single bouton afford an explanation for the interbouton variability (Reuter, 1996), identifying the mechanism and function of trial-by-trial fluctuations in a single bouton is more complex, not least because these fluctuations can occur in response to a fixed amplitude action potential and across a time course of a few seconds or less (Frenguelli and Malinow, 1996).

In this study we monitor AP-evoked  $Ca^{2+}$  transients at individual hippocampal Schaffer collateral boutons. We show that trial-by-trial variation in  $[Ca^{2+}]_i$  elevation is a feature of the  $Ca^{2+}$  signal at these sites and that  $Ca^{2+}$  transients at individual boutons fall into two distinct distributions, the smaller of the two distributions comprising the “large”  $Ca^{2+}$  transients. We perform a pharmacological analysis of the AP-evoked  $Ca^{2+}$  transients to identify the basis of these distributions. We find that the large  $Ca^{2+}$  transients occur when presynaptically located N-methyl D-aspartate receptors (NMDARs) are activated. We validate our pharmacological data by performing electron microscopy (EM) at CA3-CA1 synapses and by uncaging glutamate at synaptic boutons. In the uncaging experiment, NMDAR currents are measured at the cell soma. Crucially, presynaptic NMDAR activation facilitates synaptic transmission and appears to be tuned to produce maximum facilitation at theta frequency (~5 Hz). This is significant because theta frequency is known to be effective at inducing plasticity, such as long-term potentiation (LTP).

Because large transients occur when neurotransmitter is released, we have used the amplitude of the  $Ca^{2+}$  transients within the bouton as a novel method with which to measure  $p_r$ . We find that LTP increases the frequency of large  $Ca^{2+}$  transients, consistent with the idea that LTP increases  $p_r$ .

## RESULTS

### $[Ca^{2+}]_i$ Transients in Schaffer Collateral Boutons Are Highly Variable

Hippocampal CA3 pyramidal cells were iontophoretically injected with the  $Ca^{2+}$  indicator dyes Oregon green 488 BAPTA-1 (1 mM) and BAPTA-2 (2 mM). Figure 1A shows a projection image of a CA3 cell and Schaffer collateral axon following dye loading. To investigate AP-evoked  $Ca^{2+}$  transients within the axonal boutons, we conducted rapid line scans that allowed us

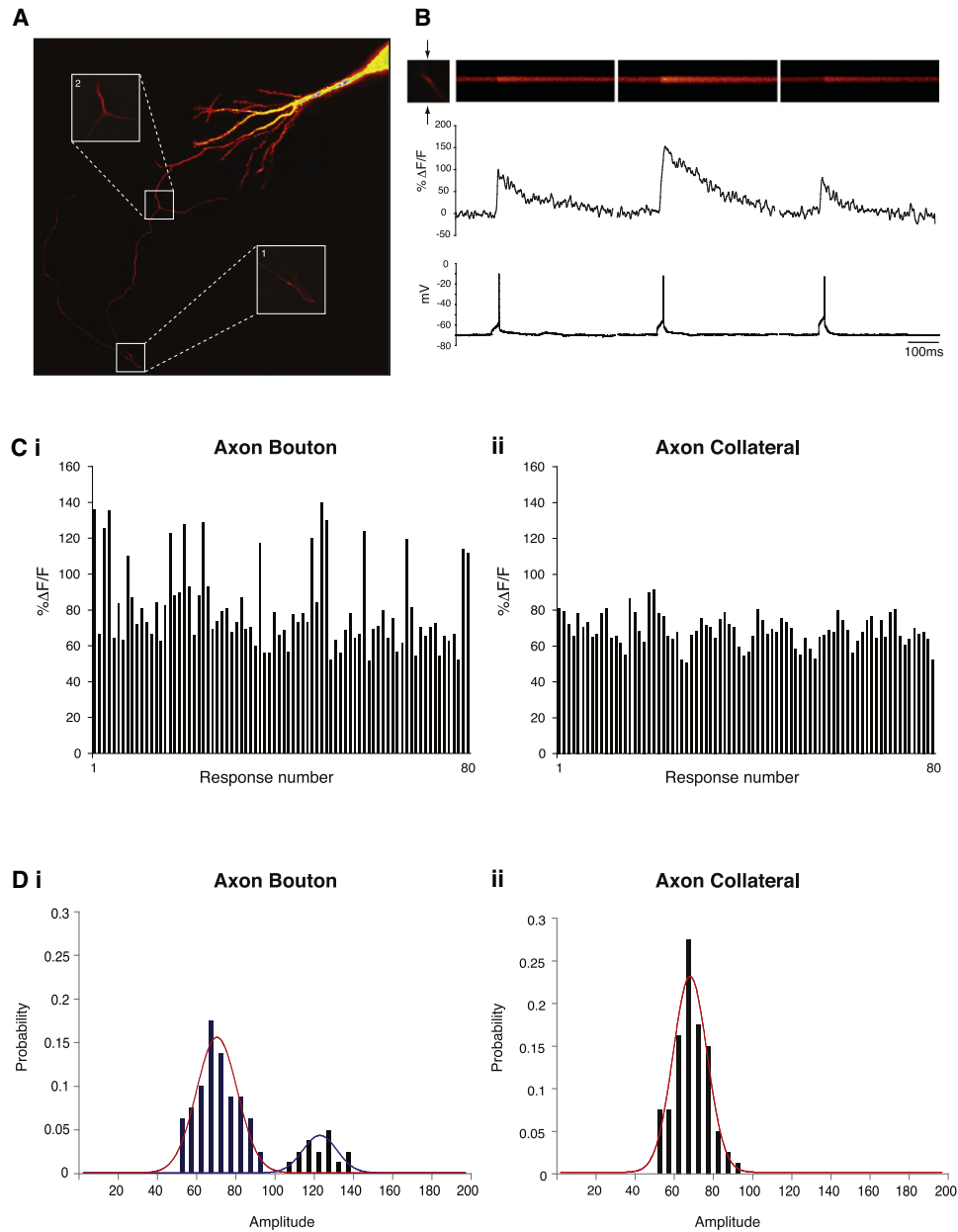


**Figure 1. Action Potential-Evoked  $\text{Ca}^{2+}$  Transients in Hippocampal Boutons Are Highly Variable**

(A) A projection confocal image of a CA3 pyramidal cell from an organotypic hippocampal slice culture iontophoretically filled with Oregon green. Presynaptic boutons along the Schaffer-axonal collaterals approximately 100–200  $\mu\text{m}$  from the soma can be readily identified as distinct varicosities. Inset panels show enlarged images of an axonal boutons (1) and axon collaterals (2).

(B) Top panel displays three line-scan images from a presynaptic bouton. Each shows an abrupt increase in  $[\text{Ca}^{2+}]_i$  near coincident with the action potential (bottom trace; mV) evoked by intrasomatic depolarizing current injection. The corresponding fractional changes in fluorescence ( $\% \Delta F/F$ ) within the bouton are variable.

(Ci and Cii) Histograms represent the  $\% \Delta F/F$  values for consecutive scans, in which the action potentials are spaced at 15 s intervals, for the bouton (Ci) and the axon collateral, 10  $\mu\text{m}$  from the bouton (Cii).

(Di and Dii) Frequency-amplitude histograms of the  $\% \Delta F/F$  values from (C). Best-fit Gaussian distributions are applied to each data set using the NORMDIST function (Microsoft Excel).

to measure the amplitude and duration of the AP-evoked  $\text{Ca}^{2+}$  current injection. The rise in  $[\text{Ca}^{2+}]_i$ , coincident with the AP (bottom trace, mV) is expressed as a fractional change in fluorescence (middle trace,  $\% \Delta F/F$ );  $\% \Delta F/F$  values for each line scan

are highly variable (Figure 1B). The rise in  $[\text{Ca}^{2+}]_i$ , coincident with the AP (bottom trace, mV) is expressed as a fractional change in fluorescence (middle trace,  $\% \Delta F/F$ );  $\% \Delta F/F$  values for each line scan

(2 ms intervals) within the scanning period (500 ms) were normalized to baseline levels and plotted on the ordinate axis. In the example shown, the peak values were 103.8, 156.3, and 84.6 in response to single APs spaced at 15 s intervals. A series of 80 APs was evoked in this way, and the  $\% \Delta F/F$  data are presented in Figure 1Ci. This protocol was repeated in the axon collateral (Figure 1Cii), so that “within cell” variability of an AP-evoked  $\text{Ca}^{2+}$  response could be compared. Figure 1A (inset panels 1 and 2) shows examples of the regions where the data illustrated in Figures 1Ci and 1Cii were collected. Whereas the amplitude of the AP-evoked  $\text{Ca}^{2+}$  transient within the bouton shows a high degree of trial-by-trial variability and can be fitted by two distinct distributions (Figure 1Di), the variability within the axon collateral is more modest and lies within a single distribution (Figure 1Dii). For ease of reference, we refer to the two distributions at the bouton as “large” and “small” events.

Although distributions can be assigned by manual data fitting, we developed an automated approach discriminate between large and small events using a Bayesian hierarchical mixture model. This method uses statistical imputation to make probabilistic state assignments (large or small events) to each measurement that accounts for experimental variation due to random and fixed effects in the modulation of the  $\text{Ca}^{2+}$  transients. The model allows us to estimate parameters such as the expected amplitudes of large and small events and the probability of observing a large event. Based on the data from each experiment, this model also delineates a threshold amplitude (red dashed line on the raw data traces), which predicts that any  $\text{Ca}^{2+}$  transient above threshold is likely to be a large rather than a small event. The estimates of parameters are expressed using 95% posterior credible intervals that report the interval in which the true parameter value lies with 95% posterior probability. Differences are deemed significant if the credible intervals are distinct and do not overlap. We also show predictive probability distributions that report estimates of the underlying distributions due to small and large events. Although the use of mixture modeling is not common, there are some important precedents (Stricker and Redman, 1994). Because our data are either uni- or bimodally distributed, we are able to move from a general case to one with model-based constraints. This adds power to our analysis, because we were able to separate out common signals from confounding factors (i.e., use of different cells, dye loading). The application of Bayesian statistics in this context is novel; we therefore provide details within the Supplemental Data.

### The Trial-by-Trial Variability of $\text{Ca}^{2+}$ Transients Is NMDAR Dependent

To understand the significance of the large  $\text{Ca}^{2+}$  events for transmitter release, we explored routes, other than influx via VDCCs, by which a  $\text{Ca}^{2+}$  rise might occur within the terminal. A number of classes of presynaptic glutamate receptor have been characterized, including kainate receptors (Lauri et al., 2001; Schmitz et al., 2003) and subtypes of metabotropic glutamate receptors (Losonczy et al., 2003; Rusakov et al., 2004; Zakharenko et al., 2002). However, for these receptor classes, the pathways thought to generate the rise in  $[\text{Ca}^{2+}]_i$  occur via signaling to the endoplasmic reticulum. In light of previous work (Emptage et al., 2001), these were unlikely to contribute to trial-by-trial vari-

ability. Consequently, we examined whether presynaptic  $[\text{Ca}^{2+}]_i$  was influenced by alternative routes of  $\text{Ca}^{2+}$  entry such as via the NMDAR. Our sampling protocol was repeated under control conditions followed by bath application of a selective NMDAR antagonist, D-AP5. After the initial line-scan protocol, 50  $\mu\text{M}$  D-AP5 was added to the artificial cerebrospinal fluid (ACSF) for 15 min in order to block NMDARs, and the line-scan protocol was repeated. Figures 2Ai and 2Aii show the  $\% \Delta F/F$  values for a single bouton before and after application of D-AP5. Blocking the NMDAR with D-AP5 abolishes large  $\text{Ca}^{2+}$  transients in the bouton. The  $\% \Delta F/F$  values by AP trial are shown for a single experiment (Figures 2Ai and 2Aii), as well as the  $\% \Delta F/F$  values for experiments on seven other boutons (eight cells; Figure 2Aiii). A series of ten  $\% \Delta F/F$  traces are overlaid in Figures 2Aiv and 2Av so that  $\tau$  may be compared. No change in  $\tau$  occurs upon application of D-AP5, although the large events (red traces) are abolished in D-AP5. The probability of observing a large event in the presence of D-AP5 is significantly reduced compared to control, as confirmed by the 95% posterior interval (ACSF  $\theta = 0.166 \pm 0.05$ ; D-AP5  $\theta = 0.005 \pm 0.009$ ;  $n = 8$ ; Figure 2Aiv). Predictive probability plots suggest that large events become small events in the presence of D-AP5. This is reflected in the complete loss of large events and the increase in the probability of observing a small event (Figure 2Av). There is no significant difference in the amplitude of small events in the presence of D-AP5 (see predictive probability distributions in Figure 2Av). In order to test whether the abolition of large  $\text{Ca}^{2+}$  events after D-AP5 application is specific to boutons, nonsynaptic regions of the axon were examined. Here the model fails to identify distinct distributions of large and small events. This is shown by the predictive probability plots in which attempts by the model to separate the data into small and large events failed to reveal a difference (Figure S1; ACSF  $\theta = 0.172 \pm 0.275$ ; D-AP5  $\theta = 0.075 \pm 0.147$ ;  $n = 5$ ; not significant).

Because NMDAR subunit composition in the hippocampus is known to vary (Sheng et al., 1994), we wished to identify whether the NR2A or NR2B subunit of the NMDAR contributed to the modulation of presynaptic  $[\text{Ca}^{2+}]_i$ . The NR2B antagonist, Ro-04-5595 (10  $\mu\text{M}$ ), was applied, and the  $\% \Delta F/F$  of AP-evoked  $\text{Ca}^{2+}$  transients was measured. The probability of observing a large event is significantly reduced in Ro-04-5595 compared to control (ACSF  $\theta = 0.253 \pm 0.08$ ; Ro-04-5595  $\theta = 0.034 \pm 0.035$ ;  $n = 5$ ; Figure 2Biv), demonstrating that receptors containing the NR2B subunit are present. Like D-AP5, the predictive probability distributions for the small events are overlaid, suggesting that there is no change in the amplitude of the small events.

### Inhibition of Presynaptic NMDARs Abolishes Trial-by-Trial Variability

Postsynaptic NMDAR activation can generate retrograde messengers such as endocannabinoids, thereby allowing modulation of transmitter release (Katona et al., 2006; Kawamura et al., 2006; Ohno-Shosaku et al., 2007). We therefore wished to examine whether the probability of observing large AP-evoked  $\text{Ca}^{2+}$  events following application of AP5 and Ro-04-5595 arose as a consequence of a postsynaptic NMDAR-mediated retrograde response. In order to achieve this, we dialyzed

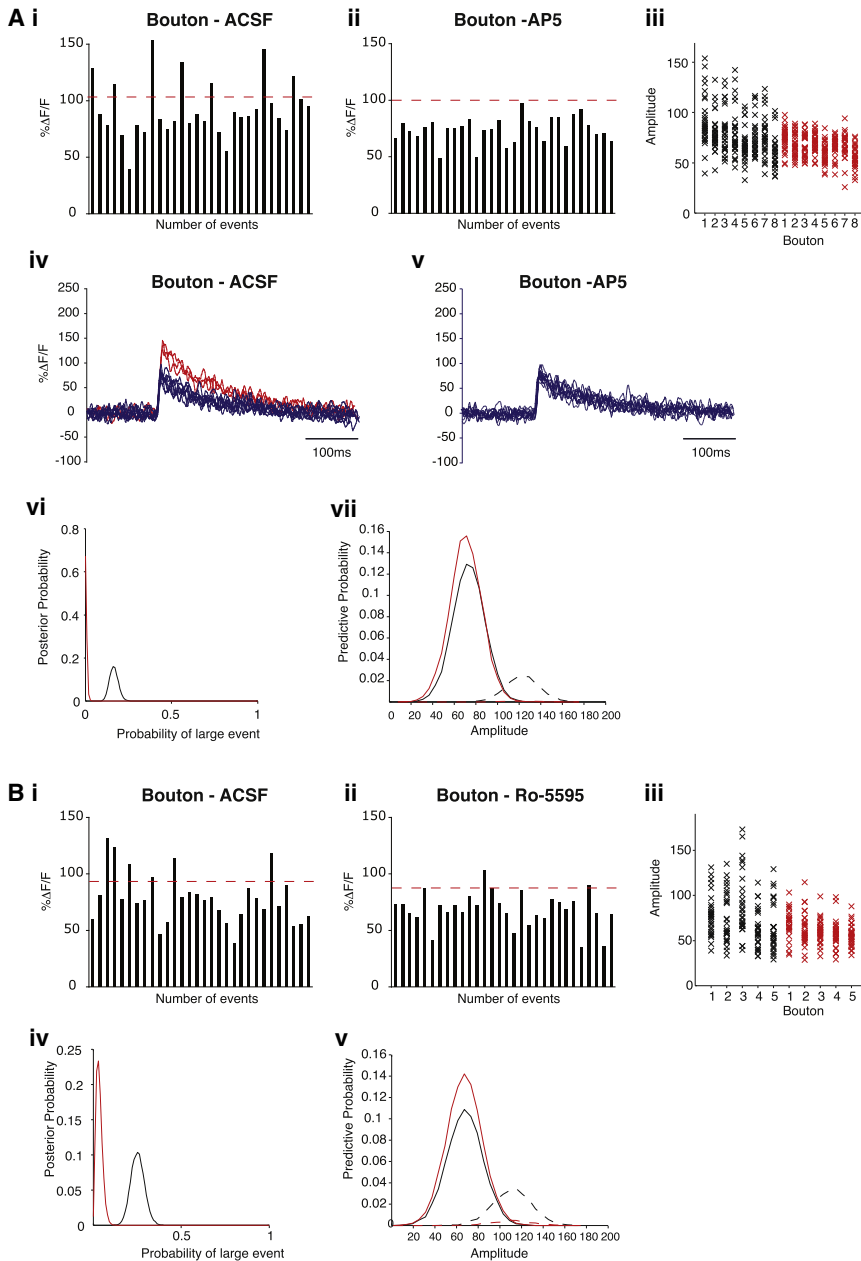


**Figure 2. Variance of Presynaptic Ca<sup>2+</sup> Transients Is NMDAR Dependent**

(A*i*-A*vii*) Histograms of %ΔF/F values for repeat line scans at boutons in control ACSF (A*i*) and in the presence of 50 μM D-AP5 (A*ii*). The dashed red line represents the threshold level, generated by our model, identifying the boundary between large and small events. Inhibition of NMDARs with D-AP5 abolishes large Ca<sup>2+</sup> transients in boutons, as seen in our trial-by-trial histogram for a single bouton (A*ii*) and for a further seven boutons, in which the all %ΔF/F values are plotted for each experiment before (black crosses) and after (red crosses) AP5 treatment (A*iii*). Ten %ΔF/F overlaid traces from bouton 2 show that τ is unchanged in D-AP5 (A*iv* and A*v*). Large events are shown by the red lines. The probability of observing a large event in the presence of D-AP5 is significantly reduced compared to control ACSF (A*vi*) (ACSF θ = 0.166 ± 0.05; D-AP5 θ = 0.005 ± 0.009; n = 8). Predictive probability plots show that the probability of observing a large event in the presence of D-AP5 falls to zero (red dashed line), whereas the probability of observing a small event increases in D-AP5 (solid red line). The amplitude distribution of small events remains unchanged in D-AP5 (A*vii*).

(B*i*-B*v*) This protocol was repeated in the presence of NR2B antagonist Ro-04-5595. Histograms are shown of %ΔF/F values for repeat line scans at boutons in control ACSF (B*i*) and in the presence of 10 μM Ro-04-5595 (B*ii*). The dashed red line represents the threshold level, as described above. Inhibition by Ro-04-5595 reduces large Ca<sup>2+</sup> transients in boutons, as seen in our trial-by-trial histogram for a single bouton (B*ii*) and for a further five boutons, in which %ΔF/F values are plotted for each experiment (B*iii*). The probability of observing a large event in the presence of Ro-04-5595 is significantly reduced compared to control ACSF (B*iv*) (ACSF θ = 0.253 ± 0.08; Ro-04-5595 θ = 0.034 ± 0.035; n = 5). Predictive probability plots show that the probability of observing a large event in the presence of Ro-04-5595 falls close to zero (red dashed line), whereas the probability of observing a small event increases in Ro-04-5595 (solid red line). The amplitude distribution of small events remains unchanged in Ro-04-5595 (B*v*).

the membrane-impermeable NMDAR antagonist norketamine directly into the presynaptic neuron via the recording electrode. We used norketamine because it binds noncompetitively to the internal face of the NMDAR (dissociation constant pK<sub>a</sub> = 7.5) and is unlikely to cross the plasma membrane (partition coefficient [log P, octanol/water], 3.1). Large AP-evoked Ca<sup>2+</sup> transients in the bouton were abolished following the introduction of norketamine compared to control (ACSF: θ = 0.173 ± 0.07; in norketamine, θ = 0.012 ± 0.019; n = 5; Figure 3A*iv*). As with D-AP5, the probability of observing a large event falls in the presence of norketamine (Figure 3A*v*), whereas the probability of observing a small event increases, but the amplitude does not change (Figure 3A*v*).

### NMDARs Are Located Both Pre- and Postsynaptically at CA3-CA1 Synapses

Our pharmacological data suggest that presynaptic NMDARs occur at Schaffer collateral boutons. We therefore sought to confirm this using alternative methods. Our first approach was to examine whether the obligatory NMDAR subunit NR1 was present at CA3 boutons by immunolabeling. To ensure that our labeling was specific, we performed these experiments in tissue from CA3-NR1 knockout (KO) mice (P21) and their control littermates (Nakazawa et al., 2002), because these offer a “within animal” control. Light micrographs show NR1 immunoreactivity present throughout the CA3 field of the control animals but absent in the CA3 area of CA3-NR1 KO (Figure 4A). Localization

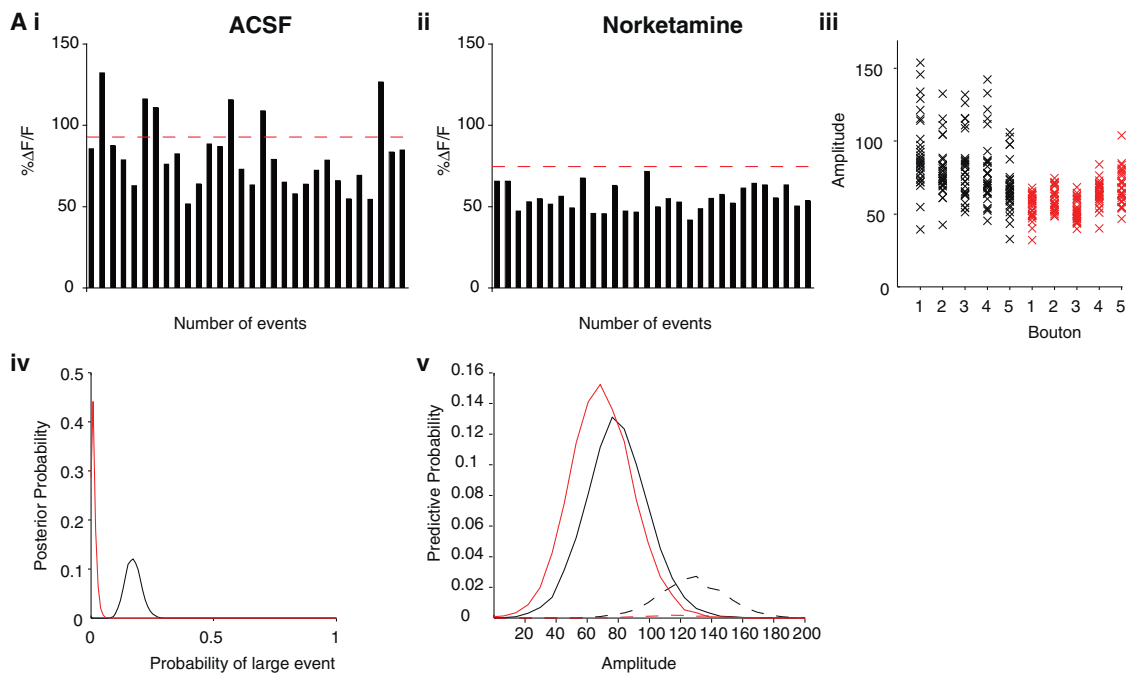


**Figure 3. Trial-by-Trial Variability of Action Potential-Evoked  $\text{Ca}^{2+}$  Transients Is Abolished by Inhibition of Presynaptic NMDARs**

(A i–A v) Ionophoretic injection of 500  $\mu\text{M}$  norketamine into the cell via an intracellular recording electrode inhibits presynaptic NMDARs. Inhibition by norketamine abolishes large  $\text{Ca}^{2+}$  transients in boutons, as seen in our trial-by-trial histogram for single boutons (A ii) and for a further four boutons, in which  $\% \Delta F/F$  values are plotted for each experiment (A iii). The dashed red line (A ii) represents the threshold level, as described above. The probability of observing a large event in the presence of norketamine is significantly reduced compared to control (A iv) (ACSF:  $\theta = 0.173 \pm 0.07$ ; in norketamine,  $\theta = 0.012 \pm 0.019$ ;  $n = 5$ ). Predictive probability plots show that the probability of observing a large event in the presence of norketamine falls to zero (red dashed line), whereas the probability of observing a small event increases in norketamine (solid red line). The amplitude distribution of small events remains unchanged in norketamine (A v).

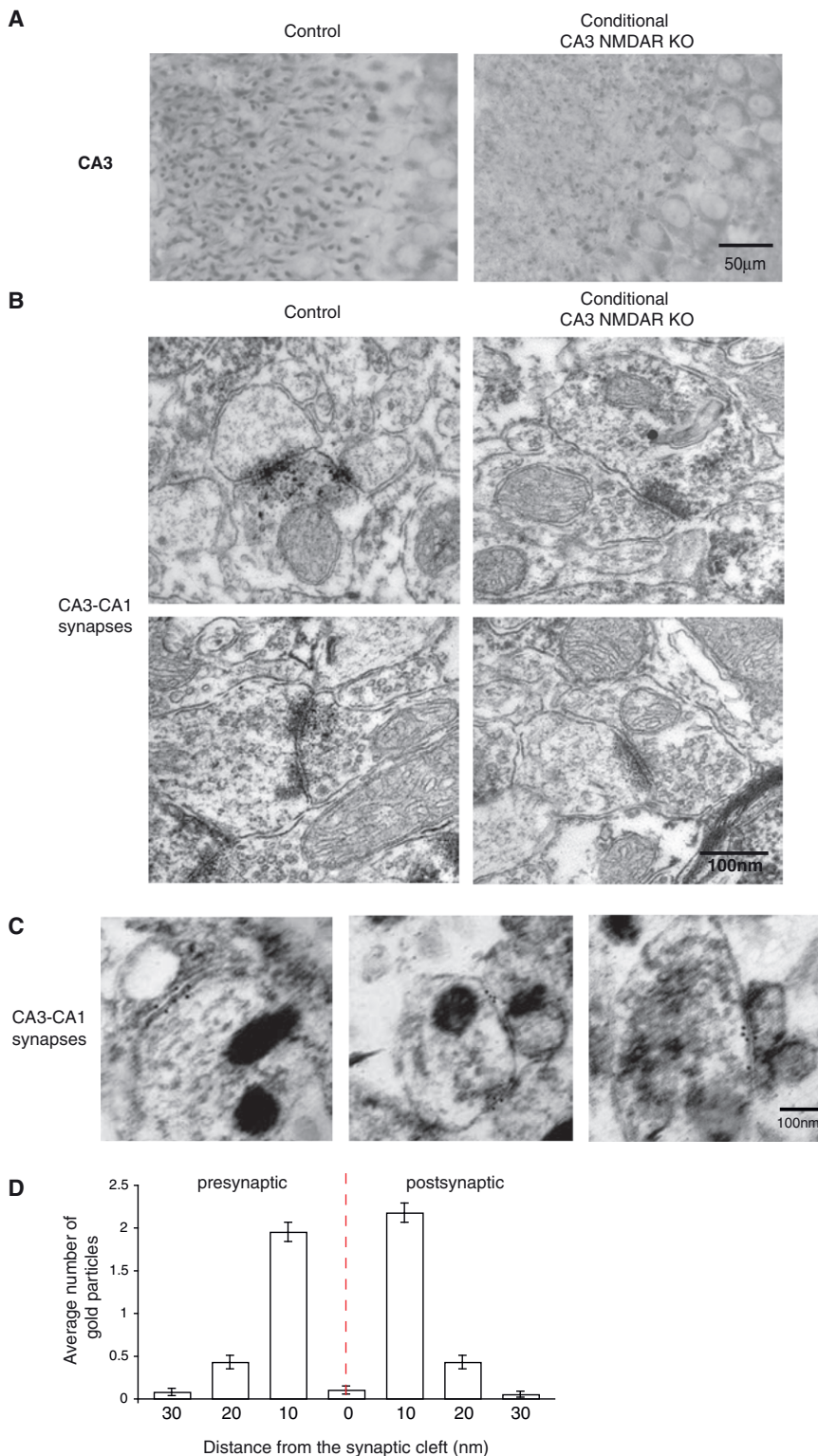
of NR1 was also conducted with electron microscopy (Figures 4B and 4C). Here, tissue quality was maintained by performing immunoperoxidase labeling. Dense patches of the DAB reaction product are readily seen both pre- and postsynaptically at CA3-CA1 synapses in control mice, whereas labeling is present exclusively in the postsynaptic region of CA3-CA1 synapses in the CA3-NR1 KO (Figure 4B).

Figure 4C shows examples of CA3-CA1 synapses from rat hippocampus (P14), each immunolabeled with 10 nm gold. Here, tissue is prepared so that receptor antigenicity is optimized. With this approach, gold particles are evident on either side of the synaptic cleft, consistent with the idea that there are both pre- and postsynaptic NMDARs. We analyzed the distribution of immunogold particles across sections from 40 synapses. No more than one section was taken from any one synapse, and no attempt was made to reconstruct a synapse in its entirety. Using this approach, we routinely identified NR1 labeling at both pre- and postsynaptic loci (Figure 3Biv), with the majority of labeling occurring within 10  $\mu\text{m}$  to either side of the synaptic cleft.

Our second approach was to apply glutamate to the bouton by performing localized photolysis of MNI-glutamate. A schematic and a description of photolytic spot calibration are provided in Figure S2A. Schaffer collateral boutons superfused in low  $\text{Mg}^{2+}$  (1 mM) ACSF to reduce the  $\text{Mg}^{2+}$  block at NMDARs. DNQX (20  $\mu\text{M}$ ), an AMPA and kainate receptor antagonist, and

MCPG (500  $\mu\text{M}$ ), a metabotropic glutamate receptor antagonist (mGluR, types I and V), were illuminated with three 4  $\mu\text{W}$ , 355 nm light pulses (1) in the presence of MNI-glutamate. Each photolytic release of glutamate produced a rapid increase in  $[\text{Ca}^{2+}]_i$  within the bouton (Figure 5Ai) that was abolished in the presence of 50  $\mu\text{M}$  D-AP5 (Figure 5Aii). Summary statistics are provided in Figure 5B (control  $\% \Delta F/F = 56.25 \pm 2.35\%$ ; D-AP5 =  $1.76 \pm 0.33$ ;  $n = 4$ ;  $p < 0.0001$ ). Illumination of boutons in the absence of MNI-glutamate produced no change in  $[\text{Ca}^{2+}]_i$  (data not shown).

Next we used photolysis of glutamate to explore presynaptic NMDAR activation kinetics and receptor distribution along the collateral. By performing rapid photolysis (single 10 ns pulses; Figure S2D),  $\text{Ca}^{2+}$  imaging, and whole-cell patch-clamp recording (Figure 5C), we were able to record pharmacologically isolated NMDAR-mediated currents following uncaging (NMDAR<sub>u</sub>) at the cell soma evoked by release at single boutons. NMDAR<sub>u</sub> currents were always accompanied by an increase in  $[\text{Ca}^{2+}]_i$  (Figure 5Di). The kinetics of the NMDAR<sub>u</sub> currents were rapid, mean time to peak of  $1.36 \pm 0.29$  ms ( $n = 6$ ; Figure 5Dii). Importantly, we only observe NMDAR<sub>u</sub> currents and their associated increase in  $[\text{Ca}^{2+}]_i$  when photolysis is directed at boutons. Directing the photolytic spot at points along the collateral failed to generate either. This is illustrated in Figures 5Ei and 5Eii, where an NMDAR<sub>u</sub> current and increase in  $[\text{Ca}^{2+}]_i$  are seen at the bouton, whereas there is no response when the spot is moved 2  $\mu\text{m}$  away from the bouton.



**Figure 4. NMDARs Are Located Both Pre- and Postsynaptically at CA3-CA1 Synapses**

(A) Light micrographs of hippocampal (p14) CA3 fields in CA3 NMDAR conditional knockout (KO) and control littermate mice DAB immunolabeled to reveal the NR1 subunit of the NMDAR. Labeling is only evident in control animals.

(B) Electron micrographs of CA3-CA1 synapses from control and NMDAR KO mice DAB immunolabeled for the NR1 subunit of the NMDAR. The NR1 subunit is located both pre- and postsynaptically in control animals and is exclusively postsynaptic in the CA3 NMDAR KO mice.

(C) Three electron micrographs of freeze-substituted rat hippocampal (p14) CA3-CA1 synapses, immunogold-labeled for NR1 (10 nm gold). NR1 labeling is present on either side of the synaptic cleft (SC). Electron-dense mitochondria are indicative of boutons.

(D) The average number of immunogold-labeled NMDARs for 40 CA3-CA1 synapses are plotted as distance from the synaptic cleft in both pre- and postsynaptic terminals (error bars  $\pm$  standard error of the mean [SEM]).

NMDAR (Mayer et al., 1984; Nowak et al., 1984), we used these features to explore the mechanism by which presynaptic NMDARs generate large  $\text{Ca}^{2+}$  transients. Initially, we increased the level of extracellular  $\text{Mg}^{2+}$  to 10 mM. Superfusion of 10 mM  $\text{Mg}^{2+}$  (Figures 6Aii and 6Aiii) significantly reduced the probability of observing a large event (ACSF  $\theta = 0.185 \pm 0.075$ ; 10 mM  $\text{Mg}^{2+}$   $\theta = 0.009 \pm 0.018$ ;  $n = 5$ ; Figures 6Aii–6Aiv), whereas the amplitude of these events remains unchanged (Figure 6Av). In contrast, the absence of  $\text{Mg}^{2+}$  from the extracellular solution did not change the probability of observing a large  $\text{Ca}^{2+}$  event (ACSF  $\theta = 0.19 \pm 0.079$ ;  $\text{Mg}^{2+}$ -free  $\theta = 0.197 \pm 0.078$ ;  $n = 5$ ; Figure 6Biv) but did increase the amplitude of both large and small events (Figure 6Bv).

We manipulated the release of glutamate from the boutons by modifying the duration of the AP. This was achieved by lowering the extracellular concentration of  $\text{K}^+$  ions to 0.1 mM, thereby reducing the duration of the AP, or by applying 4-aminopyridine (4-AP, 40  $\mu\text{M}$ ) to increase AP duration (Qian and Saggau, 1999). As expected, low  $\text{K}^+$  conditions significantly decreased the width of the AP (ACSF:  $\tau$  [ms] =  $2.35 \pm 0.01$ ;

0.1 mM  $\text{K}^+$ :  $\tau = 1.65 \pm 0.01$ ;  $n = 4$ ;  $p < 0.0001$ ). With the duration of the AP reduced, the probability of observing large  $\text{Ca}^{2+}$  events was significantly decreased compared to control (ACSF

**Presynaptic NMDARs Are Autoreceptors**

Because both voltage-dependent relief of the  $\text{Mg}^{2+}$  block and glutamate binding are requisite steps for the activation of the

$\theta = 0.178 \pm 0.075$ ;  $0.1 \text{ mM K}^+ \theta = 0.134 \pm 0.043$ ;  $n = 4$ ; Figure 7Aiv). In contrast, 4-AP enhanced spike duration (ACSF:  $\tau$  [ms] =  $2.14 \pm 0.07$ ;  $40 \mu\text{M}$  4-AP:  $\tau = 14.36 \pm 2.7$ ;  $n = 5$ ;  $p < 0.0001$ ) and significantly increased the probability of observing a large event (ACSF  $\theta = 0.196 \pm 0.063$ ;  $40 \mu\text{M}$  4-AP  $\theta = 0.006 \pm 0.013$ ;  $n = 5$ ; Figure 7Biv). These results indicate that in normal  $\text{K}^+$  conditions, the depolarization arising from a single AP invading the bouton is adequate to relieve the  $\text{Mg}^{2+}$  block of the NMDAR, but this is not the case when the AP duration is curtailed. Enhancing the duration of the AP increases  $\text{Ca}^{2+}$  influx and consequently transmitter release (Mintz et al., 1995; Wu and Saggau, 1994b); thus, the increase in the incidence of large events is consistent with the idea that glutamate release is required for their production.

Any one of a number of sources of glutamate might activate presynaptic NMDARs. However, because the incidence of large transients was reminiscent of the stochastic pattern of transmitter release, we decided to block AP-evoked glutamate release and assess whether this changed the probability of observing large  $\text{Ca}^{2+}$  transients. Blocking neurotransmission by application of bafilomycin A1 (Figures 8Aii and 8Aiii) significantly reduced the probability of observing a large  $\text{Ca}^{2+}$  event (ACSF  $\theta = 0.18 \pm 0.067$ ; Baf A1  $\theta = 0.008 \pm 0.016$ ;  $n = 5$ ; Figure 8Aiv), suggesting that AP-evoked glutamate release is critical for the generation of large  $\text{Ca}^{2+}$  events and that presynaptic NMDARs are activated when an AP triggers this release. To guard against off-target effects, we repeated the experiment by blocking neurotransmission with Botulinum toxin (BoTx) type C (500 nM). Dialysis of BoTx via micropipette into CA3 cells significantly reduced the probability of observing a large  $\text{Ca}^{2+}$  event in boutons (ACSF  $\theta = 0.186 \pm 0.067$ ; BoTx  $\theta = 0.008 \pm 0.017$ ;  $n = 4$ ; Figures 8Bi–8Biv), again consistent with the idea that transmitter release is necessary for the generation of large  $\text{Ca}^{2+}$  events.

In light of these data, we propose a model that describes the way in which large  $\text{Ca}^{2+}$  transients arise from NMDAR activation (Figure 9). (1) AP invasion into the terminal depolarizes the membrane. The duration of a somatically recorded AP in hippocampal neurons is  $\sim 2.5$ – $3$  ms (Qian and Saggau, 1999; Gong et al., 2008). (2) Depolarization opens VDCCs, which elevates  $[\text{Ca}^{2+}]_i$  and produces a small  $\text{Ca}^{2+}$  transient in the bouton. The time taken to open VDCCs is  $\sim 0.2$  ms (Lee et al., 2000; Randall and Tsien, 1995), and the time taken for diffusion of  $\text{Ca}^{2+}$  from VDCCs to synaptic vesicles is estimated to be  $\sim 0.3$  ms (Meinrenken et al., 2002). (3) When release occurs, the time taken for exocytosis is  $\sim 0.3$  ms (Bruns and Jahn, 1995; Meinrenken et al., 2002). Glutamate must then diffuse to the NMDARs. Previous studies report diffusion coefficient values in the range  $D = 0.3$ – $0.76 \mu\text{m}^2/\text{ms}$  (Savtchenko and Rusakov, 2004; Ventriglia and Di Maio, 2000). For diffusion to occur across the width of a bouton ( $0.5$ – $1 \mu\text{m}$ ), we estimate the transition time ( $t_{tr}$ ) to be between  $0.05$  and  $0.5$  ms. This is determined by assuming that glutamate performs a random walk in which mean square deviation (MSD) is described by  $\text{MSD} = 6 \cdot D \cdot t_{tr}$ . By summing each of these parameters, we estimate that glutamate will arrive at the presynaptic NMDARs within  $1.3$  ms. (4) Because glutamate arrival occurs during the envelope of depolarization of the AP, relief of the  $\text{Mg}^{2+}$  block is concurrent with the arrival of glutamate.

The kinetics of  $\text{Mg}^{2+}$  unblock are reported to be very fast, around  $100$ – $200 \mu\text{s}$  (Jahr and Stevens, 1990; Kampa et al., 2004), so  $\text{Mg}^{2+}$  relief looks unlikely to be rate limiting. Once activated, the average time of the NMDAR current to peak is  $\sim 1.36$  ms (see Figure 5). (5)  $\text{Ca}^{2+}$  influx via NMDARs will sum with residual  $\text{Ca}^{2+}$  from VDCC-mediated entry, producing the large  $\text{Ca}^{2+}$  transient. Our model assumes that because large events occur following transmitter release, further release will not occur. However, the subsequent arrival of an AP, in which the interspike interval is less than the clearance rate of  $\text{Ca}^{2+}$ , will result in facilitation of transmitter release.

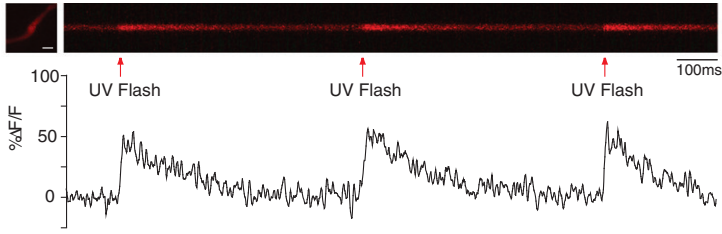
### Facilitation of Transmitter Release at Theta Frequency Is Mediated by Presynaptic NMDARs

The functional significance of activation of presynaptic NMDARs for transmitter release has not been explored. To assess this, we stimulated neurons at different frequencies and examined release under conditions in which large  $\text{Ca}^{2+}$  transients occur and are abolished with D-AP5. The readout for release is the peak amplitude of the AMPAR-mediated EPSC, because this is a measure of the level of transmitter release under conditions in which postsynaptic NMDARs contribute minimally to the current recorded (Durand et al., 1996; Kauer et al., 1988; Liao et al., 1995). Three frequencies were examined:  $1$ ,  $5$ , or  $20$  Hz in trains of ten pulses. The amplitude of EPSCs for each condition was normalized to the first response in the train. Analysis was conducted by performing a two-factor, repeated-measures analysis of variance on a mean of ten train repetitions across ten cells. As would be predicted, the response under control conditions and in the presence of  $50 \mu\text{M}$  D-AP5 to single stimuli or to the first stimulus in a train remained unchanged. Similarly, the delivery of a  $1$  Hz train did not significantly affect the size of the EPSC across ten pulses ( $p = 0.118$ ), nor did the addition of D-AP5 affect the EPSC ( $p = 0.319$ ; Figure 10A). However, Figure 10B shows that a  $5$  Hz train produced significant facilitation of the EPSC ( $p < 0.0001$ ) that was abolished by D-AP5 ( $p < 0.05$ ). A further increase in frequency to  $20$  Hz again produced significant facilitation of the EPSC ( $p < 0.0001$ ); however, application of D-AP5 did not change the magnitude of facilitation ( $p = 0.191$ ; Figure 10C). A summary showing the amplitude ratio of the first and fifth EPSC for each frequency reveals the extent to which stimulation at  $5$  Hz is NMDA autoreceptor dependent.

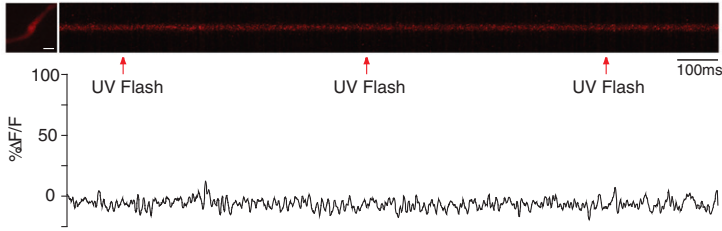
### $p_r$ Determines the Incidence of Large $\text{Ca}^{2+}$ Events

From our data, we propose that the incidence of large  $\text{Ca}^{2+}$  events is directly linked to the stochastic pattern of transmitter release (Figure 9). Because  $p_r$  is heterogeneous across boutons (Emptage et al., 2003; Kirischuk and Grantyn, 2002; Schikorski and Stevens, 2001; Ward et al., 2006), the model is readily testable, because the incidence of large transients should be independent for each bouton, even along a single axon. Furthermore, the incidence of large  $\text{Ca}^{2+}$  transients should change in response to manipulations known to change  $p_r$ , such as adenosine (Asztely et al., 1994; Emptage et al., 1999; Wu and Saggau, 1994a) or the induction of LTP (Antonova et al., 2001; Bolshakov and Siegelbaum, 1995; Emptage et al., 2003; Enoki et al., 2009; Malgaroli et al., 1995; Ward et al., 2006).

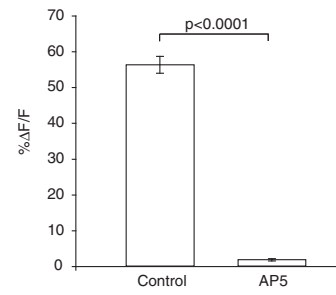
**A(i)** + DNQX + MCPG



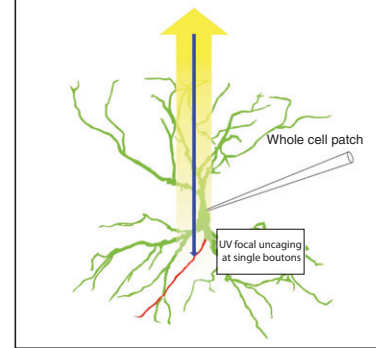
**(ii)** + DNQX + MCPG + AP5



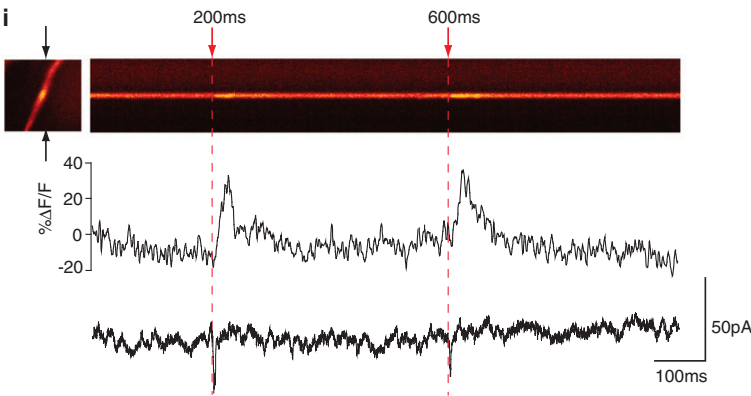
**B**



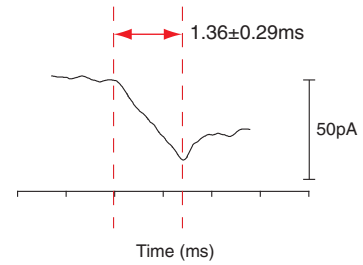
**C** Single bouton Ca<sup>2+</sup> imaging



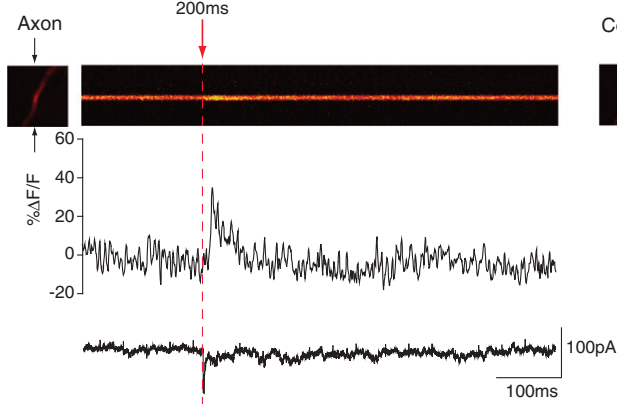
**D i**



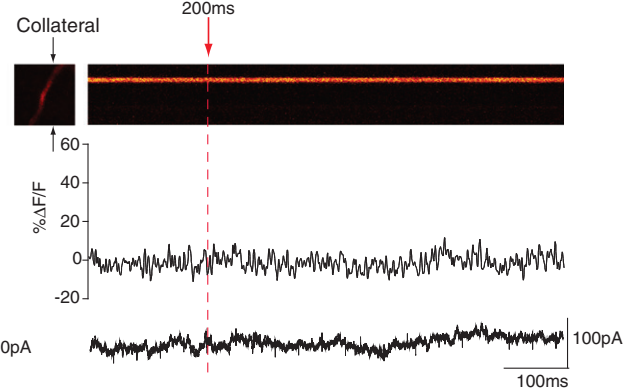
**ii**



**E i**



**ii**



Line scans were performed along axon collaterals where more than one bouton was traversed. APs were evoked and  $\text{Ca}^{2+}$  transient amplitudes were measured and analyzed at each of the boutons. Each of the 40 APs is temporally matched, i.e., the same AP evokes the  $\text{Ca}^{2+}$  transient measured in each bouton. Figure 11A demonstrates that the AP-evoked  $\text{Ca}^{2+}$  transient amplitude varies independently between boutons separated by just a few microns following a single AP propagating along the collateral. AP-evoked  $\text{Ca}^{2+}$  transients in bouton 1 show large transients at times when bouton 2 shows small transients.

Does manipulation of  $p_r$  change the incidence of large AP-evoked  $\text{Ca}^{2+}$  transients? For this we applied the neuromodulator adenosine, known to act presynaptically to reduce  $p_r$ . Addition of adenosine reduced, but did not abolish, all large  $\text{Ca}^{2+}$  transients (Figures 11Bii and 11Biii), as confirmed by a reduction in the probability of observing a large  $\text{Ca}^{2+}$  event (ACSF  $\theta = 0.139 \pm 0.05$ ; adenosine  $\theta = 0.065 \pm 0.033$ ;  $n = 5$ ; Figure 11Biv; summarized in Figure 11C).

Finally, we induced LTP using theta frequency stimulation. The induction of LTP increases the frequency of large  $\text{Ca}^{2+}$  transients at boutons (Figures 12Ai and 12Aii). We observed an increase in the probability of obtaining a large  $\text{Ca}^{2+}$  event at six out of ten boutons following a single LTP-inducing stimulus (control  $\theta = 0.134 \pm 0.064$ ; LTP1  $\theta = 0.184 \pm 0.07$ ) and a further increase in the number of large events at four out of four boutons following a further round of LTP induction (LTP2  $\theta = 0.232 \pm 0.076$ ;  $n = 4$ ; Figure 12Bii). In contrast, the amplitude of the large  $\text{Ca}^{2+}$  events in presynaptic boutons does not change after the induction of LTP (Figure 12Biii).

## DISCUSSION

The variance of AP-evoked  $\text{Ca}^{2+}$  transients between boutons of the same axon collateral has been reported in a number of regions of the CNS including cortical neurons (Frenguelli and Malinow, 1996; Koester and Sakmann, 2000; Mackenzie et al., 1996), cerebellar basket cells (Llano et al., 1997), superior collicular neurons (Kirschuk and Grantyn, 2002), and hippocampal pyramidal neurons (Wu and Saggau, 1994b). Moreover, variance within a single bouton has been described in layer V cortical neurons (Frenguelli and Malinow, 1996). Here we describe vari-

ability of  $\text{Ca}^{2+}$  transient amplitudes at single Schaffer collateral boutons of CA3 neurons and demonstrate that the variability arises from presynaptic NMDARs. Despite a wealth of data about hippocampal NMDARs, almost nothing is known of their localization to, or role within, the presynaptic bouton. Here we demonstrate that NMDARs are present within boutons and that their activation is dependent on AP-evoked release of glutamate; that is, they act as autoreceptors. Once activated, the  $\text{Ca}^{2+}$  influx via NMDARs adds to the influx via VDCCs, producing a large  $\text{Ca}^{2+}$  transient and thereby increasing the probability that transmitter release will occur to a subsequent AP. Enhancement of release appears to be “tuned” to operate optimally at theta frequency, because excitatory postsynaptic potential (EPSP) facilitation at this frequency is abolished by inhibition of presynaptic NMDAR activation. Theta frequency is a significant oscillatory rhythm in rodents, because it is observed during exploratory behavior and is highly effective in the induction of LTP (Frick et al., 2004; Hoffman et al., 2002; Kelso and Brown, 1986; Watanabe et al., 2002). The facilitatory action of presynaptic NMDARs on neurotransmission offers a mechanistic rationale as to why theta frequency is effective for LTP induction. These data also resolve the paradox of how it is that synapses with low  $p_r$  are able to contribute to the induction of LTP. A synapse with a  $p_r$  of 0.1 might be expected to release transmitter just twice during a train of 20 APs and might therefore be expected to fail to achieve adequate activation of the postsynaptic neuron. However, the feedback loop generated from  $\text{Ca}^{2+}$  influx via activation of NMDA autoreceptors will ensure that a low  $p_r$  synapse achieves augmented release during the course of the stimulus train (Figure 10B).

The relationship between transmitter release and presynaptic NMDAR activation also has utility, because manipulations of  $p_r$  also change the probability of observing presynaptic NMDAR-mediated large  $\text{Ca}^{2+}$  events. Manipulations that reduce  $p_r$ , boutons, such as adenosine, decrease the number of large  $\text{Ca}^{2+}$  events, whereas manipulations that increase  $p_r$  increase the number of large events. Importantly, induction of LTP, which is reported to increase  $p_r$  at active synapses (Antonova et al., 2001; Bolshakov and Siegelbaum, 1995; Emptage et al., 2003; Enoki et al., 2009; Malgaroli et al., 1995; Ward et al., 2006), increases the incidence of large  $\text{Ca}^{2+}$  transients. Therefore, the measurement of the number of large  $\text{Ca}^{2+}$  transients in the

### Figure 5. Focal Uncaging of MNI-Glutamate at Presynaptic Boutons Elicits $\text{Ca}^{2+}$ Transients

(Ai and Aii) Top panel shows an example of a line-scan image collected at a Schaffer collateral bouton during focal uncaging of glutamate. 355 nm light pulses ( $\uparrow$ ) applied to the bouton in the presence of MNI-glutamate (2.5 mM) produced a rapid increase in  $[\text{Ca}^{2+}]_i$  (Ai). The corresponding fractional change in fluorescence ( $\%F/F$ ) within the bouton for each uncaging event is presented in the bottom panel. The uncaging protocol was repeated in the presence of D-AP5, where photolysis did not evoke  $\text{Ca}^{2+}$  transients (Aii).

(B) A histogram provides summary data of the  $\% \Delta F/F$   $\text{Ca}^{2+}$  response produced by glutamate uncaging in four experiments under control and D-AP5 conditions (error bars  $\pm$  SEM).

(C) Individual Schaffer collateral boutons ( $<100 \mu\text{m}$  from the cell soma) are illuminated with single 20 ns pulses of 355 nm light in the presence of MNI glutamate (2.5 mM).  $\text{Ca}^{2+}$  indicator dyes report glutamate-evoked elevations in intracellular  $\text{Ca}^{2+}$  at the bouton. NMDARs were pharmacologically isolated by bathing the tissue in DNQX and MCPG. Extracellular  $\text{Mg}^{2+}$  levels were reduced to 0.5 mM. Whole-cell patch electrode recordings were made concurrently with the glutamate photolysis/ $\text{Ca}^{2+}$  imaging.

(Di) Photolytic release of glutamate at a single bouton at 200 ms and again at 600 ms produced a  $\text{Ca}^{2+}$  transient within the bouton and an NMDAR-mediated current at the cell soma.

(Dii) An average of NMDAR currents from six boutons reveals that the time to peak following the first photolytic event (200 ms) is  $1.36 \pm 0.29$  ms.

(Ei and Eii) An example of the photolytic release of glutamate eliciting an NMDAR-mediated  $\text{Ca}^{2+}$  transient and somatic current when delivered to the bouton, but not when delivered to an adjacent ( $\sim 2 \mu\text{m}$ ) section of axon collateral.

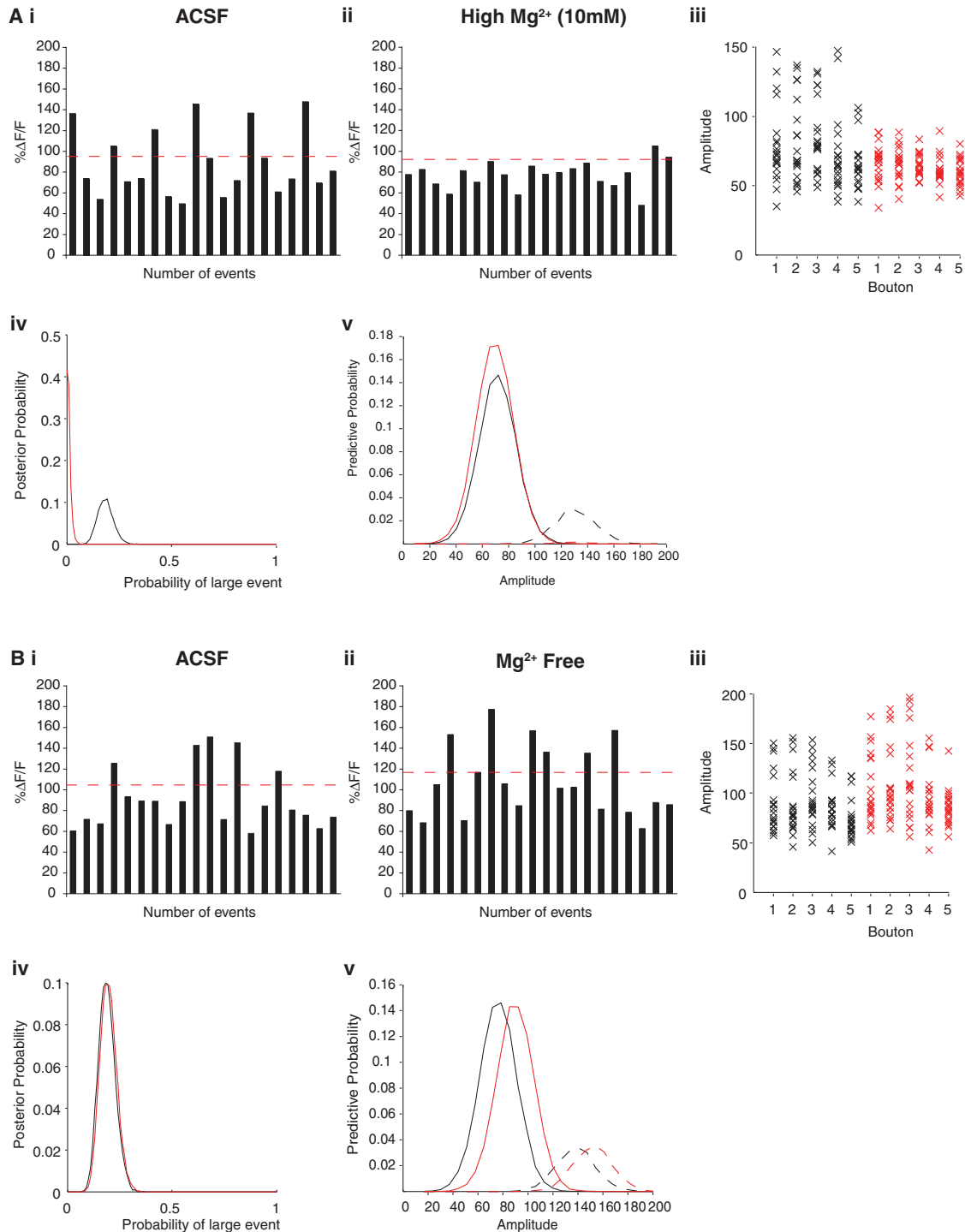


**Figure 6.  $[Mg^{2+}]_o$  Influences the Probability of Observing a Large Event**

(A–Av) Superfusion of 10 mM  $Mg^{2+}$  ACSF significantly reduced the probability of observing a large  $Ca^{2+}$  event. Inhibition by high (10 mM)  $[Mg^{2+}]_o$  abolishes large  $Ca^{2+}$  transients in boutons, as seen in our trial-by-trial histogram for single boutons (Aii) and for a further four boutons, in which  $\% \Delta F/F$  values are plotted for each experiment (Aiii). The dashed red line (Aii) represents the threshold level, as described above. The probability of observing a large event in the presence of high  $[Mg^{2+}]_o$  is significantly reduced compared to control (Aiv) (ACSF  $\theta = 0.185 \pm 0.075$ ; 10 mM  $Mg^{2+}$   $\theta = 0.009 \pm 0.018$ ;  $n = 5$ ). Predictive probability plots show that the probability of observing a large event in the presence of (10 mM)  $[Mg^{2+}]_o$  falls to zero (red dashed line), whereas the probability of observing a small event increases in (10 mM)  $[Mg^{2+}]_o$  (solid red line). The amplitude distribution of small events remains unchanged in (10 mM)  $[Mg^{2+}]_o$  (Av).

(B–Bv) Superfusion of  $Mg^{2+}$ -free ACSF for 10 min to relieve the  $Mg^{2+}$  block did not change the probability of observing large events. Relief of the  $Mg^{2+}$  block produces no change in the probability of observing a large  $Ca^{2+}$  transient in boutons, as seen in our trial-by-trial histogram for single boutons (Bii) and for a further

bouton provides a novel technique with which to measure  $p_r$ . Whether this approach has utility at other axon terminals will be dependent on the presence of NMDAR autoreceptors. There is an interesting correlation in the literature that would seem to suggest that  $\text{Ca}^{2+}$  transient variability at the presynaptic boutons and presynaptic NMDARs is a general motif. For example, (1) modulating the frequency of mini EPSPs in the entorhinal cortex (Berretta and Jones, 1996; Woodhall et al., 2001), layer V of the visual cortex (Sjöström et al., 2003), or CA1 pyramidal neurons of the hippocampus (Madara and Levine, 2008) or (2) enhancing long-term depression (LTD) in the visual cortex (Sjöström et al., 2003), the barrel cortex (Rodríguez-Moreno and Paulsen, 2008), and the cerebellum (Duguid and Smart, 2004) all require presynaptic NMDAR activation and each are regions known to show highly variable presynaptic  $\text{Ca}^{2+}$  transients (Frenguelli and Malinow, 1996; Kirischuk and Grantyn, 2002; Llano et al., 1997; Wu and Saggau, 1994b).

The recognition that large  $\text{Ca}^{2+}$  transients occur as part of a process that is likely to be mechanistically distinct from AP-elicited influx of  $\text{Ca}^{2+}$  via VDCCs alone required an unambiguous method of identifying large versus small events. We have developed a statistical approach enabling us to separate large and small events using a blind procedure.

Application of the NMDAR antagonists significantly reduced the probability of observing large  $\text{Ca}^{2+}$  events, providing the first indication that presynaptic NMDARs contributed to the  $\text{Ca}^{2+}$  signal measured in the bouton. Interestingly, inhibition of NR2B containing NMDARs does not produce a result significantly different from that observed in D-AP5. Because the NMDAR subunit composition is reported to change during development, with the number of NR2A-containing NMDARs thought to increase and perhaps partly replace NR2B-containing receptors within the synapse (Flint et al., 1997; Monyer et al., 1994; Stocca and Vicini, 1998), our data suggest that we are examining terminals still at an early stage in development.

There is literature describing the distribution of NMDAR subunits in the brain, including the hippocampus. NMDAR subunits have been identified at both the pre- and postsynaptic locus. Of relevance here is that although NR1 subunits are reported to localize at CA1 dendrites (Petralia et al., 1994) and in dendritic spines (Petralia and Wenthold, 1999; Racca et al., 2000; Takumi et al., 1999), they have not been reported in boutons. In contrast, NR2B subunits have been shown to localize in presynaptic terminals of primate hippocampal CA3-CA1 synapses (Janssen et al., 2005), and NR2B and NR2D subunits have been found in presynaptic terminals of rat CA3-CA1 synapses (Charton et al., 1999; Thompson et al., 2002) and within the dentate molecular layer (Jourdain et al., 2007). Here we take the immunoEM literature a step further by showing that the NR1 subunit is also present.

NMDAR activation is classically dependent on both the presence of glutamate and the depolarization-induced relief of the

$\text{Mg}^{2+}$  block, so we manipulated each of these factors independently in our study. The results inform us that the receptor behaves in a classical way, but they additionally reveal that large transients arise from transmitter release; thus, the variance in  $\text{Ca}^{2+}$  transient amplitude is a direct consequence of the stochastic nature of transmitter release and, as such, can be used as a proxy for  $p_r$ .

Although our pharmacological manipulations are consistent with presynaptic NMDARs having an autoreceptor role, we were mindful that the arrival of glutamate at the receptor must coincide with depolarization of the membrane; in essence, this means that the events we observe must be initiated within the duration of a single AP. To assess this, we measured the time required for the NMDAR current to reach its peak following rapid release of glutamate at a bouton. We observe rapid activation kinetics, within the range in which presynaptic NMDARs could function as autoreceptors. Rise time constants in this range for NMDAR have been reported previously (Kampa et al., 2004; Steinert et al., 2010). We therefore have no reason to advocate anything unique about the kinetic performance of hippocampal presynaptic NMDARs.

Focal release of caged glutamate was also used to explore whether NMDAR currents might be detected outside the region of the bouton. Because we find this to not be the case, it appears that the receptor density is highest at boutons. This result is important because it indicates that the large amplitude  $\text{Ca}^{2+}$  transients we observe at boutons do not arise as an anomaly of  $\text{Ca}^{2+}$  imaging, dyes, or cellular buffers, but are a robust measure of  $\text{Ca}^{2+}$  influx at that site.

Direct evidence for NMDA autoreceptors in the hippocampus is new; however, evidence linking NMDAR autoregulatory release in plasticity is described in other brain areas. Presynaptic NMDARs are implicated in the modulation of LTD in the visual cortex (Sjöström et al., 2003), cerebellum (Casado et al., 2002; Duguid and Smart, 2004), and barrel cortex (Rodríguez-Moreno and Paulsen, 2008). Interestingly, little evidence exists linking presynaptic NMDARs to LTP. In fact, Rodríguez-Moreno and Paulsen (2008) report that in barrel cortex, the type of plasticity expressed, LTD or LTP, is linked to whether pre- or postsynaptic NMDARs are activated. Our data suggest that presynaptic NMDARs serve to facilitate transmission at theta frequency and are therefore likely to augment the induction of LTP.

Analysis of  $\text{Ca}^{2+}$  transients evoked by single spikes provides little information about the stimulus conditions under which augmentation of the  $\text{Ca}^{2+}$  signal might alter transmitter release. We therefore measured transmitter release in response to different stimulus frequencies. We found that presynaptic NMDAR activation produced robust facilitation of transmission during theta frequency and that although stimulation at higher frequencies also facilitates the amplitude of the postsynaptic current, the facilitation is insensitive to D-AP5. Presynaptic

---

four boutons, in which  $\% \Delta F/F$  values are plotted for each experiment (Biii). The dashed red line (Bii) represents the threshold level, as described above. The probability of observing a large event in the absence of  $\text{Mg}^{2+}$  is not reduced as compared to control (Biv) (ACSF  $\theta = 0.19 \pm 0.079$ ;  $\text{Mg}^{2+}$ -free  $\theta = 0.197 \pm 0.078$ ;  $n = 5$ ). Predictive probability plots show that the probability of observing a large event in the absence of  $\text{Mg}^{2+}$  is unchanged (red dashed line). The amplitude distribution of both large and small events increases (rightward shift) in the absence of  $\text{Mg}^{2+}$  (Bv).

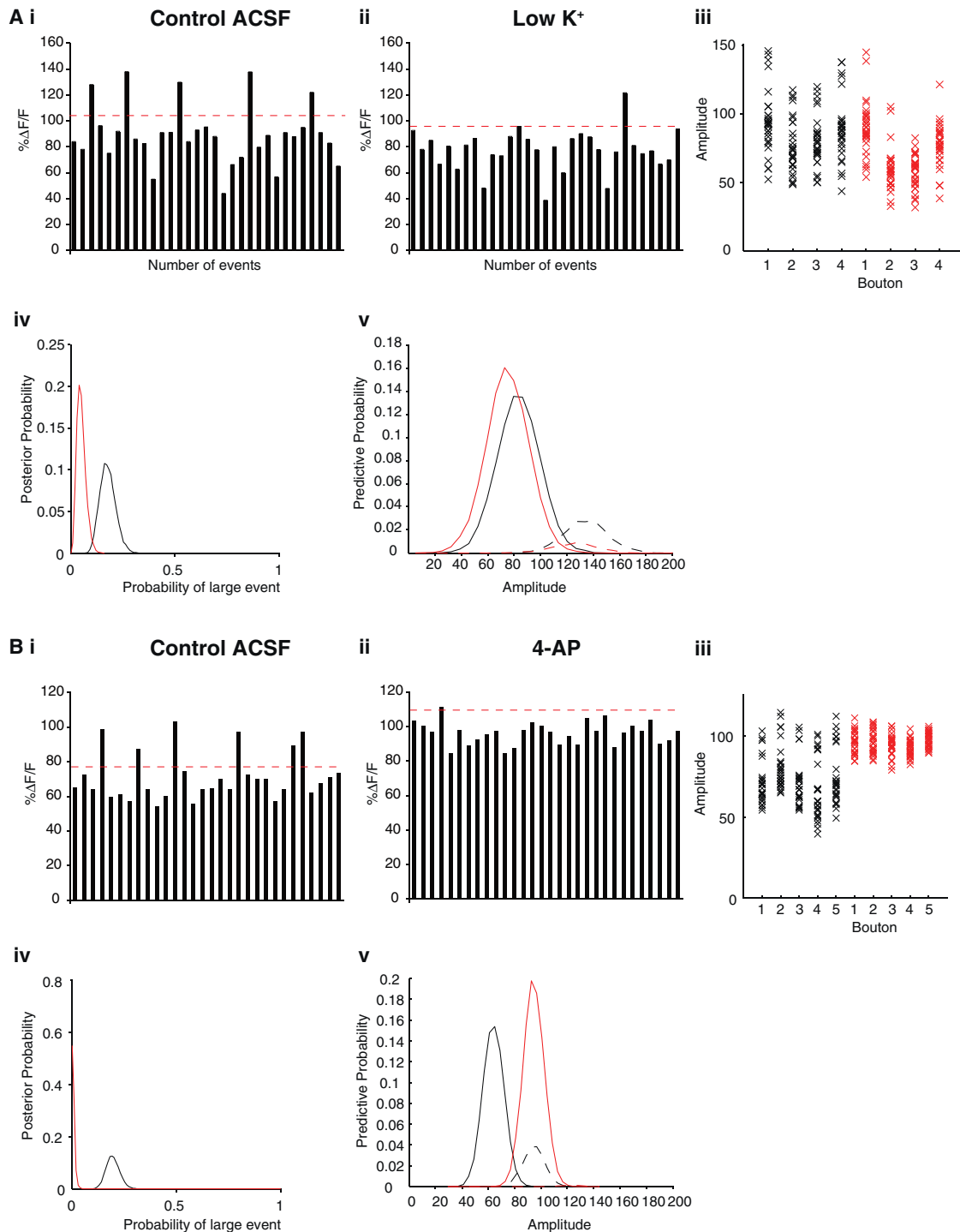


**Figure 7. Modulation of Transmitter Release by AP Duration Influences the Probability of Observing a Large Event**

(Ai–Av) Superfusion of low- $K^+$  (0.1 mM) ACSF significantly reduced both the duration of the AP (ACSF:  $\tau = 2.35 \pm 0.01$ ; 0.1 mM  $K^+$ :  $\tau = 1.65 \pm 0.01$ ;  $n = 4$ ;  $p < 0.0001$ , paired Student's  $t$  test) and the probability of observing a large  $Ca^{2+}$  event. Inhibition by low  $K^+$  abolishes large  $Ca^{2+}$  transients in boutons, as seen in our trial-by-trial histogram for single boutons (Aii) and for a further three boutons, in which % $\Delta F/F$  values are plotted for each experiment (Aiii). The dashed red line (Aii) represents the threshold level, as described previously. The probability of observing a large event in the presence of low  $K^+$  is significantly reduced compared to control (Aiv) (ACSF  $\theta = 0.178 \pm 0.075$ ; 0.1 mM  $K^+$   $\theta = 0.134 \pm 0.043$ ;  $n = 4$ ). Predictive probability plots show that the probability of observing a large event in low  $K^+$  falls to zero (red dashed line), whereas the probability of observing a small event increases in low  $K^+$  (solid red line). The amplitude distribution of small events remains unchanged in low  $K^+$  (Av).

NMDARs serve to augment transmitter release at theta frequency, but when the frequency of APs reaches 20 Hz,  $\text{Ca}^{2+}$  entry through VDCCs occurs with such rapidity that the bouton becomes progressively more  $\text{Ca}^{2+}$  loaded, that is,  $\text{Ca}^{2+}$  entry exceeds clearance.

### Large $\text{Ca}^{2+}$ Transients as a Reporter of $p_r$

Our search to understand the basis of  $\text{Ca}^{2+}$  transient variance serendipitously led us to identify a novel way to measure  $p_r$ . We therefore sought to verify that large  $\text{Ca}^{2+}$  events signaled transmitter release. We show that large events, like  $p_r$ , are heterogeneous between boutons. This has additional significance because it illustrates that the electrotonic spread of NMDAR-mediated depolarization elicited in the dendrites, as reported for cerebellar interneurons (Christie and Jahr, 2008), cannot be responsible for the NMDAR-mediated large  $\text{Ca}^{2+}$  transients seen here, because large events occur at some boutons but not others along the same axon in response to the same AP. Furthermore, the amplitude of transients does not scale with increased distance from the soma: a large event can occur at a distant bouton concurrent with a small event at a bouton close to the soma. We also show that large events decrease in number following the addition of adenosine or increase following addition of 4-AP. We utilized this new technique to test whether  $p_r$  changes after the induction of LTP, as we and others have previously reported (Antonova et al., 2001; Bolshakov and Siegelbaum, 1994; Enoki et al., 2009; Malgaroli et al., 1995; Zakharenko et al., 2001). We find that LTP produces an increase in the incidence of large  $\text{Ca}^{2+}$  events at some but not all boutons to a single round of LTP (Figure 12C). A second round of LTP increased  $p_r$  at boutons that had previously not shown an increase or increased further the incidence of large  $\text{Ca}^{2+}$  events at boutons that had previously shown an increase. These data are consistent with previous work in which LTP produces an increase in  $p_r$  at active synapses (Emptage et al., 2003; Enoki et al., 2009) but does not show an increase in  $p_r$  at silent synapses (Emptage et al., 2003; Ward et al., 2006). However, silent synapses once unmasked by LTP do show an increase in  $p_r$ . These data also reveal that multiple rounds of LTP are able to repeatedly increase  $p_r$  at active synapses. This not only illustrates how heterogeneity of  $p_r$  might be achieved but also has implications for information storage, because it illustrates that synapses are not bistable elements but instead serve as graded storage devices capable of repeatedly updating transmission efficacy.

## EXPERIMENTAL PROCEDURES

### Hippocampal Organotypic Slice Cultures

Transverse 350  $\mu\text{m}$  hippocampal organotypic slices were prepared from male Wistar rat pups, postnatal day 7 (Harlan UK) as previously described (Emptage et al., 1999; Stoppini et al., 1991). Each slice was maintained in culture for 7–14 days prior to use.

### Electrophysiology and Imaging

Slices were transferred to a recording chamber (Scientific Systems Design) mounted on an Olympus BX50WI microscope with a BioRad Radiance 2000 confocal scanhead (BioRad/Zeiss) and were superfused at 30°C with oxygenated ACSF as described previously (Ward et al., 2006). Whole-cell patch clamp and sharp microelectrode recording techniques were used in the study, and the data were collected using WIN WCP software (Strathclyde Electrophysiology Software). The criteria employed for identifying axons and boutons has previously been characterized using synaptophysin staining (Emptage et al., 2001). In brief, the Oregon green 488 fluorescence allowed the identification of axons according to the following criteria: thin shaft (as opposed to dendrites), tortuous trajectory, and distinct varicosities in the absence of dendritic spines. The boutons selected were located 75–300  $\mu\text{m}$  and at least two branch points distal to the initial axon segment for pharmacological characterization. Line scans were synchronized to intrasomatically stimulated APs triggered by injecting current ( $\sim 0.5$ – $2.5 \mu\text{A}$ ) with a stimulus duration of 30  $\mu\text{s}$ . At least 40 action potentials, evoked at 15 s intervals, were sampled both before and after manipulation. AP-evoked  $\text{Ca}^{2+}$  transients in boutons were captured using Laser Sharp Software and (measured over their initial 10 ms) were expressed as fractional change in fluorescence,  $\% \Delta F/F = 100 \times (F - F_{\text{initial}}) / (F_{\text{initial}} - F_{\text{background}})$ . For details of experimental solutions and stimulus paradigms, please consult the [Supplemental Experimental Procedures](#).

### UV Spot Photolysis

355 nm photolysis was achieved using a frequency-tripled Lumonics HY 600 laser operating at 20 Hz and producing 10 ns pulses. Beam power was controlled with a series of three polarizing prisms. Experiments were performed with a laser power of 4  $\mu\text{W}$  delivered to the back aperture of the objective lens. Temporal control was achieved using an external shutter. A beam expander comprising two planoconvex lenses was used to back-fill the objective lens. The UV beam was coupled into the confocal microscope light path by way of beam-steering mirrors, a focusing lens to adjust parafocality, and a custom-made band-stop dichroic mirror centered at 360 nm (Chroma Technology). All other optical components were supplied by Thorlabs. A schematic of the apparatus used to perform photolysis is shown in Figure S2A.

We confirmed that our system was capable of achieving photolysis within a focal volume comparable to that of an individual bouton with 2.5 mM CMNB caged fluorescein (Invitrogen). Details can be found in Figure S2B.

### Electron Microscopy

Two protocols were used in the preparation of the brain tissue for immunolabeling and electron microscopy. We adapted the published procedure of Peddie et al., 2008 for the pre-embedding immunoperoxidase staining. Here we sought to preserve tissue morphology. We also prepared tissue by slam-freezing followed by flat embedding prior to immunolabeling where we wished to preserve tissue antigenicity for immunogold labeling. The full details of each procedure are provided in the [Supplemental Experimental Procedures](#).

### Statistical Analysis

All data have been analyzed using the Bayesian hierarchical mixture model analysis, unless otherwise stated.

## SUPPLEMENTAL INFORMATION

Supplemental Information includes two figures, Supplemental Data, and Supplemental Experimental Procedures and can be found online at doi: [10.1016/j.neuron.2010.11.023](https://doi.org/10.1016/j.neuron.2010.11.023).

(Bi–Bv) 4-AP (40  $\mu\text{M}$ ) significantly broadened the AP ( $\tau$  consistently 5 $\times$  control) and significantly increased the probability of observing a large  $\text{Ca}^{2+}$  transient, as seen in our trial-by-trial histogram for a single bouton (Bii) and for a further four boutons, in which  $\% \Delta F/F$  values are plotted for each experiment (Biii). The dashed red line (Bi) represents the threshold level, as described previously. The probability of observing a large event in the presence of 4-AP is significantly increased compared to control (Biv) (ACSF  $\theta = 0.196 \pm 0.063$ ; 4-AP  $\theta = 0.006 \pm 0.013$ ;  $n = 5$ ). Predictive probability plots show that the probability of observing a large event in 4-AP increases (solid red line), whereas the probability of observing a small event decreases (red dashed line) (Bv).

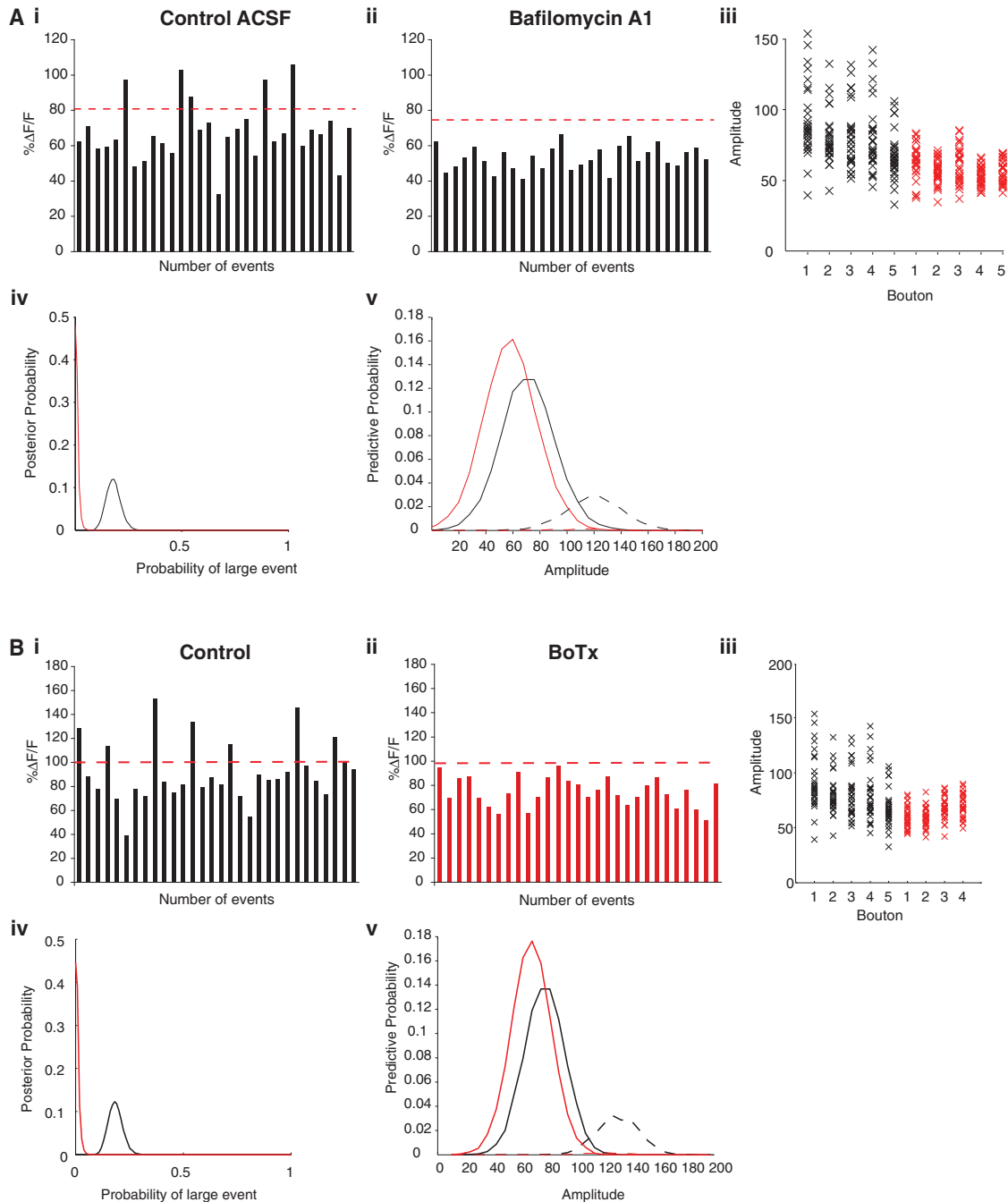


**Figure 8. Activation of the Presynaptic NMDAR Requires Vesicular Glutamate Release**

(A1–A5) Bafilomycin A1 abolishes large  $\text{Ca}^{2+}$  transients in boutons, as seen in our trial-by-trial histogram for single boutons (Aii) and for a further four boutons, in which  $\% \Delta F/F$  values are plotted for each experiment (Aiii). The dashed red line (Ai and Aii) represents the threshold level, as described previously. The probability of observing a large event in the presence of bafilomycin A1 is significantly reduced compared to control (ACSF  $\theta = 0.18 \pm 0.067$ ; Baf A1  $\theta = 0.008 \pm 0.016$ ;  $n = 5$ ) (Aiv). Predictive probability plots (Av) show that the probability of observing a large event in the presence of bafilomycin A1 falls to zero (red dashed line), whereas the probability of observing a small event increases in bafilomycin A1 (solid red line).

(B1–B5) Introduction of 500 nM Botulinum toxin (BoTx) type C via microinjection into CA3 pyramidal cells inhibits synaptic transmission and abolishes large  $\text{Ca}^{2+}$  transients in boutons, as seen in our trial-by-trial histogram for single boutons (Bii) and for a further three boutons, in which  $\% \Delta F/F$  values are plotted for each experiment (Biii). The dashed red line (Bi and Bii) represents the threshold level. The probability of observing a large event in the presence of BoTx is significantly reduced compared to control (ACSF  $\theta = 0.186 \pm 0.067$ ; BoTx  $\theta = 0.008 \pm 0.017$ ;  $n = 4$ ) (Biv). Predictive probability plots (Bv) show that the probability of observing a large event in the presence of BoTx falls to zero (red dashed line), whereas the probability of observing a small event increases in BoTx (solid red line).

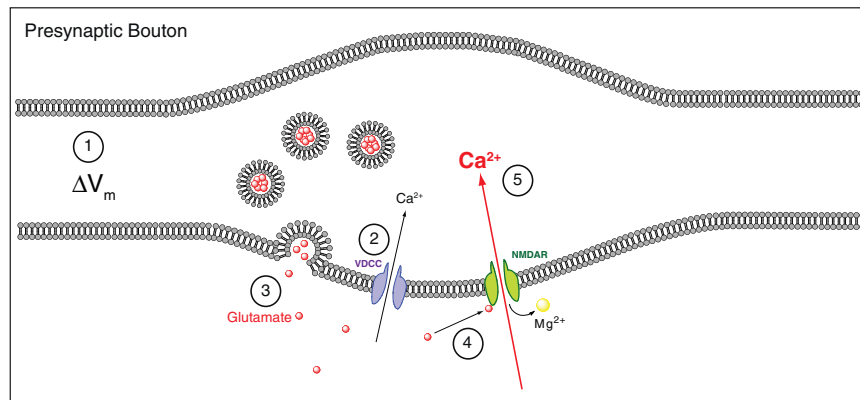


**Figure 9. A Model to Illustrate the Sequence of Events by which NMDA Autoreceptors Augment  $\text{Ca}^{2+}$  Entry to Produce Large Transients**

A description of the model is provided within the text.

## ACKNOWLEDGMENTS

We are enormously indebted to Thomas McHugh (RIKEN) for providing us with the CA3-NR1 KO mice for this study. We also wish to thank Ian Williams for assistance with perfusions and Tim Bliss for critically reading the manuscript. We are grateful for funding support from the Medical Research Council (UK).

Accepted: October 1, 2010

Published: December 21, 2010

## REFERENCES

- Antonova, I., Arancio, O., Trillat, A.C., Wang, H.G., Zablow, L., Udo, H., Kandel, E.R., and Hawkins, R.D. (2001). Rapid increase in clusters of presynaptic proteins at onset of long-lasting potentiation. *Science* 294, 1547–1550.
- Asztely, F., Xiao, M.Y., Wigström, H., and Gustafsson, B. (1994). Effect of adenosine-induced changes in presynaptic release probability on long-term potentiation in the hippocampal CA1 region. *J. Neurosci.* 14, 6707–6714.
- Augustine, G.J. (2001). How does calcium trigger neurotransmitter release? *Curr. Opin. Neurobiol.* 11, 320–326.
- Berretta, N., and Jones, R.S. (1996). Tonic facilitation of glutamate release by presynaptic N-methyl-D-aspartate autoreceptors in the entorhinal cortex. *Neuroscience* 75, 339–344.
- Bolshakov, V.Y., and Siegelbaum, S.A. (1994). Postsynaptic induction and presynaptic expression of hippocampal long-term depression. *Science* 264, 1148–1152.
- Bolshakov, V.Y., and Siegelbaum, S.A. (1995). Regulation of hippocampal transmitter release during development and long-term potentiation. *Science* 269, 1730–1734.
- Borst, J.G., and Sakmann, B. (1996). Calcium influx and transmitter release in a fast CNS synapse. *Nature* 383, 431–434.
- Bruns, D., and Jahn, R. (1995). Real-time measurement of transmitter release from single synaptic vesicles. *Nature* 377, 62–65.
- Casado, M., Isoppe, P., and Ascher, P. (2002). Involvement of presynaptic N-methyl-D-aspartate receptors in cerebellar long-term depression. *Neuron* 33, 123–130.
- Charton, J.P., Herkert, M., Becker, C.M., and Schröder, H. (1999). Cellular and subcellular localization of the 2B-subunit of the NMDA receptor in the adult rat telencephalon. *Brain Res.* 816, 609–617.
- Christie, J.M., and Jahr, C.E. (2008). Dendritic NMDA receptors activate axonal calcium channels. *Neuron* 60, 298–307.
- Dodge, F.A., Jr., and Rahamimoff, R. (1967). Co-operative action a calcium ions in transmitter release at the neuromuscular junction. *J. Physiol.* 193, 419–432.
- Duguid, I.C., and Smart, T.G. (2004). Retrograde activation of presynaptic NMDA receptors enhances GABA release at cerebellar interneuron-Purkinje cell synapses. *Nat. Neurosci.* 7, 525–533.
- Durand, G.M., Kovalchuk, Y., and Konnerth, A. (1996). Long-term potentiation and functional synapse induction in developing hippocampus. *Nature* 381, 71–75.
- Emptage, N., Bliss, T.V., and Fine, A. (1999). Single synaptic events evoke NMDA receptor-mediated release of calcium from internal stores in hippocampal dendritic spines. *Neuron* 22, 115–124.
- Emptage, N.J., Reid, C.A., and Fine, A. (2001). Calcium stores in hippocampal synaptic boutons mediate short-term plasticity, store-operated  $\text{Ca}^{2+}$  entry, and spontaneous transmitter release. *Neuron* 29, 197–208.
- Emptage, N.J., Reid, C.A., Fine, A., and Bliss, T.V. (2003). Optical quantal analysis reveals a presynaptic component of LTP at hippocampal Schaffer-associational synapses. *Neuron* 38, 797–804.
- Enoki, R., Hu, Y.L., Hamilton, D., and Fine, A. (2009). Expression of long-term plasticity at individual synapses in hippocampus is graded, bidirectional, and mainly presynaptic: Optical quantal analysis. *Neuron* 62, 242–253.
- Flint, A.C., Maisch, U.S., Weishaupt, J.H., Kriegstein, A.R., and Monyer, H. (1997). NR2A subunit expression shortens NMDA receptor synaptic currents in developing neocortex. *J. Neurosci.* 17, 2469–2476.
- Frequelli, B.G., and Malinow, R. (1996). Fluctuations in intracellular calcium responses to action potentials in single en passage presynaptic boutons of layer V neurons in neocortical slices. *Learn. Mem.* 3, 150–159.
- Frick, A., Magee, J., and Johnston, D. (2004). LTP is accompanied by an enhanced local excitability of pyramidal neuron dendrites. *Nat. Neurosci.* 7, 126–135.
- Gong, B., Liu, M., and Qi, Z. (2008). Membrane potential dependent duration of action potentials in cultured rat hippocampal neurons. *Cell. Mol. Neurobiol.* 28, 49–56.
- Hoffman, D.A., Sprengel, R., and Sakmann, B. (2002). Molecular dissection of hippocampal theta-burst pairing potentiation. *Proc. Natl. Acad. Sci. USA* 99, 7740–7745.
- Jahr, C.E., and Stevens, C.F. (1990). A quantitative description of NMDA receptor-channel kinetic behavior. *J. Neurosci.* 10, 1830–1837.
- Janssen, W.G., Vissavajhala, P., Andrews, G., Moran, T., Hof, P.R., and Morrison, J.H. (2005). Cellular and synaptic distribution of NR2A and NR2B in macaque monkey and rat hippocampus as visualized with subunit-specific monoclonal antibodies. *Exp. Neurol.* 191 (Suppl 1), S28–S44.
- Jourdain, P., Bergersen, L.H., Bhaukaurally, K., Bezzi, P., Santello, M., Domercq, M., Matute, C., Tonello, F., Gunderson, V., and Volterra, A. (2007). Glutamate exocytosis from astrocytes controls synaptic strength. *Nat. Neurosci.* 10, 331–339.

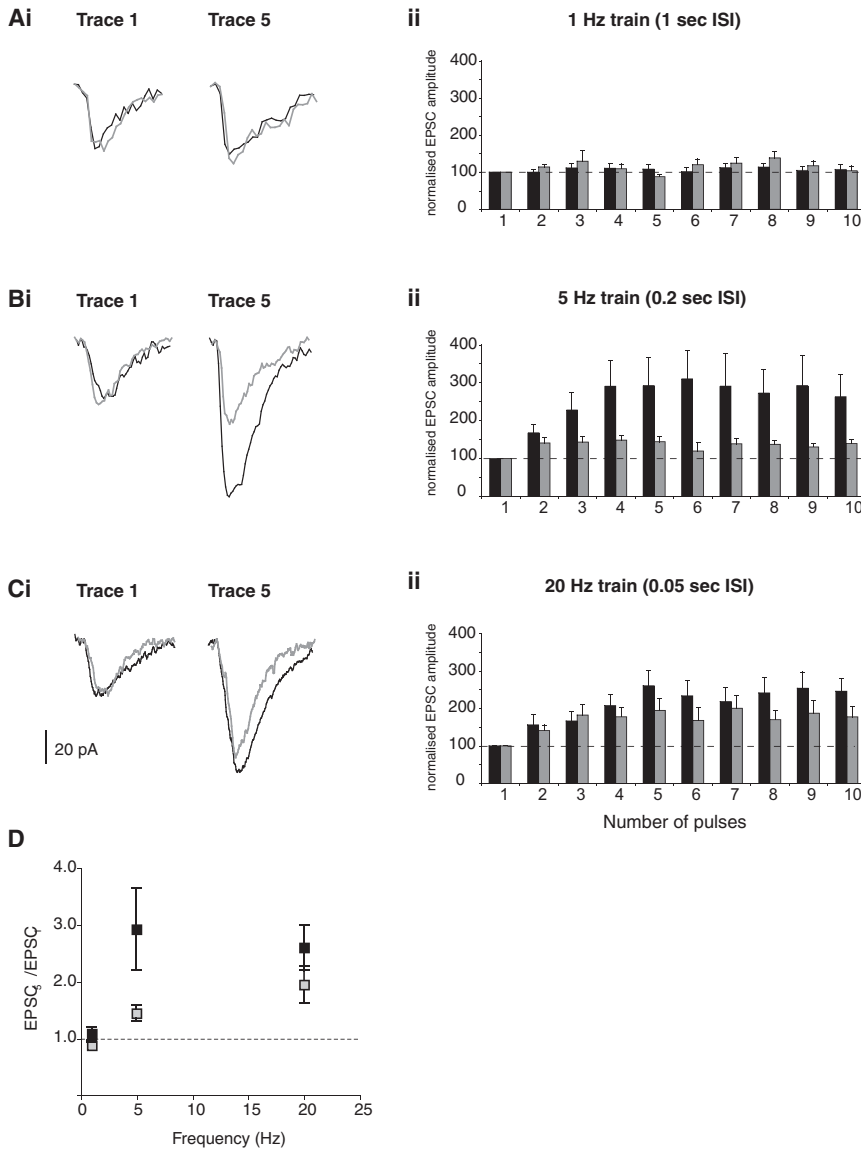


**Figure 10. Presynaptic Facilitation Mediated by NMDA Autoreceptors Is Frequency Dependent**

(Ai–Cii) The amplitude of synaptically evoked currents in ACSF (black) and 50  $\mu$ M D-AP5 (gray) are plotted as histograms (Aii, Bii, and Cii). The currents are normalized to the first response for a 1, 5, or 20 Hz train of ten stimuli (mean of ten train repetitions across ten cells,  $\pm$  standard error of the mean). Sample currents are also shown (Ai, Bi, and Ci). D-AP5 (50  $\mu$ M) significantly blocked presynaptic facilitation at 5 Hz ( $p < 0.05$ ), but not at 1 Hz or 20 Hz (1 Hz:  $p = 0.118$ ; 20 Hz:  $p = 0.191$ ; analysis of variance).

(D) EPSC ratios for the first and fifth EPSC in the trains are shown for each stimulus frequency for both control and D-AP5 conditions (error bars  $\pm$  SEM).

Kampa, B.M., Clements, J., Jonas, P., and Stuart, G.J. (2004). Kinetics of Mg<sup>2+</sup> unblock of NMDA receptors: Implications for spike-timing dependent synaptic plasticity. *J. Physiol.* 556, 337–345.

Katona, I., Urbán, G.M., Wallace, M., Ledent, C., Jung, K.M., Piomelli, D., Mackie, K., and Freund, T.F. (2006). Molecular composition of the endocannabinoid system at glutamatergic synapses. *J. Neurosci.* 26, 5628–5637.

Katz, B., and Miledi, R. (1970). Further study of the role of calcium in synaptic transmission. *J. Physiol.* 207, 789–801.

Kauer, J.A., Malenka, R.C., and Nicoll, R.A. (1988). A persistent postsynaptic modification mediates long-term potentiation in the hippocampus. *Neuron* 1, 911–917.

Kawamura, Y., Fukaya, M., Maejima, T., Yoshida, T., Miura, E., Watanabe, M., Ohno-Shosaku, T., and Kano, M. (2006). The CB1 cannabinoid receptor is the major cannabinoid receptor at excitatory presynaptic sites in the hippocampus and cerebellum. *J. Neurosci.* 26, 2991–3001.

Kelso, S.R., and Brown, T.H. (1986). Differential conditioning of associative synaptic enhancement in hippocampal brain slices. *Science* 232, 85–87.

Kirischuk, S., and Grantyn, R. (2002). Inter-bouton variability of synaptic strength correlates with heterogeneity of presynaptic Ca<sup>2+</sup> signals. *J. Neurophysiol.* 88, 2172–2176.

Koester, H.J., and Sakmann, B. (2000). Calcium dynamics associated with action potentials in single nerve terminals of pyramidal cells in layer 2/3 of the young rat neocortex. *J. Physiol.* 529, 625–646.

Lauri, S.E., Bortolotto, Z.A., Bleakman, D., Ornstein, P.L., Lodge, D., Isaac, J.T., and Collingridge, G.L. (2001). A critical role of a facilitatory presynaptic kainate receptor in mossy fiber LTP. *Neuron* 32, 697–709.

Lee, A., Scheuer, T., and Catterall, W.A. (2000). Ca<sup>2+</sup>/calmodulin-dependent facilitation and inactivation of P/Q-type Ca<sup>2+</sup> channels. *J. Neurosci.* 20, 6830–6838.

Liao, D., Hessler, N.A., and Malinow, R. (1995). Activation of postsynaptically silent synapses during pairing-induced LTP in CA1 region of hippocampal slice. *Nature* 375, 400–404.

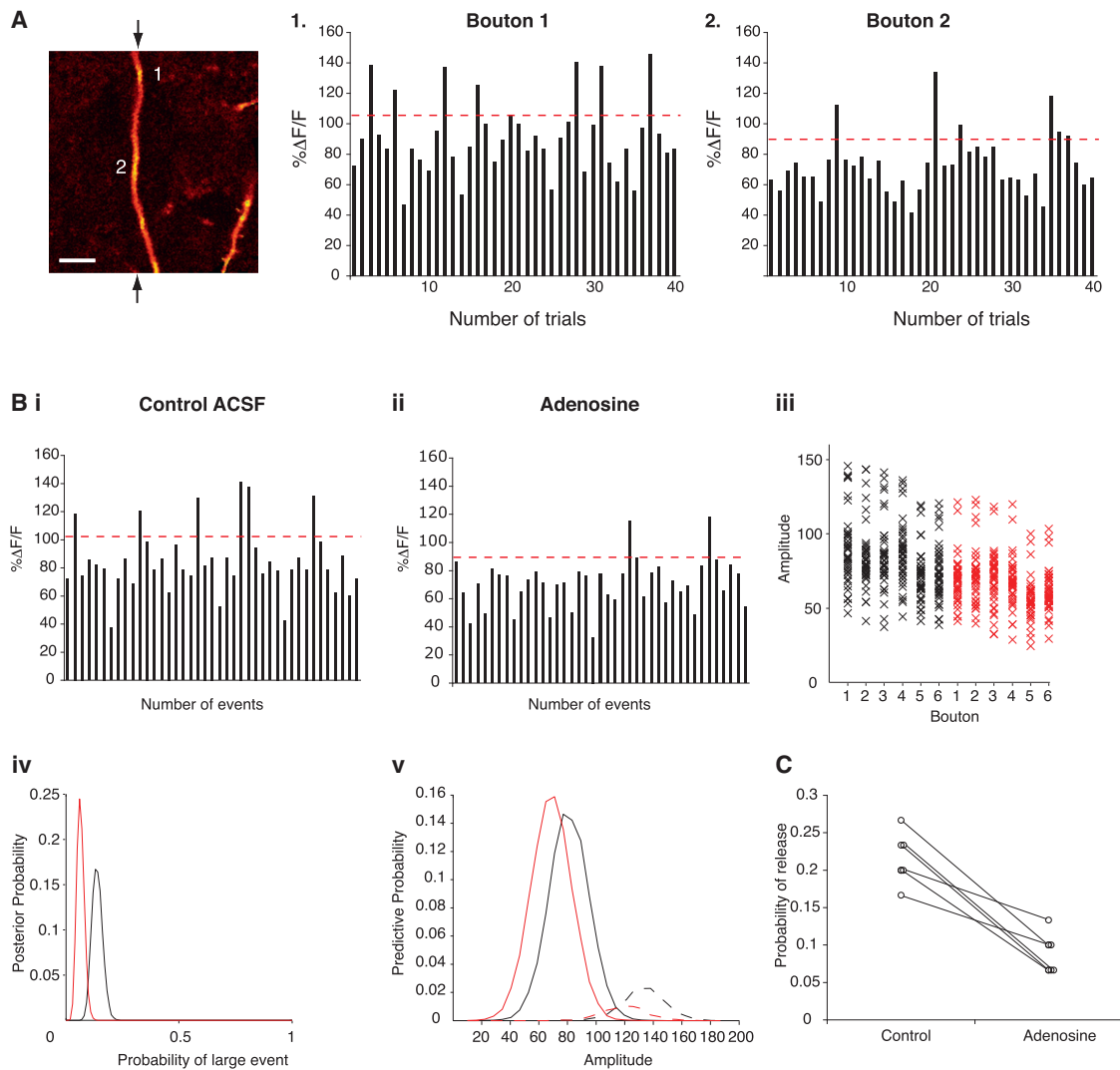


**Figure 11. The Incidence of Large  $\text{Ca}^{2+}$  Events Is Heterogeneous between Boutons and Can Be Manipulated by Modulators of  $p_r$ .** (A) Confocal image of an axon collateral approximately  $100\ \mu\text{m}$  from the soma of a CA3 pyramidal neuron filled with Oregon green 488 BAPTA-1. Arrows indicate the trajectory of the line scan for the data illustrated (scale bar =  $10\ \mu\text{m}$ ). Histograms of  $\% \Delta F/F$  values for two adjacent boutons are shown. The data were collected simultaneously in response to single APs elicited by intrasomatic current injection. The dashed red line represents the threshold level, as described previously. (B*i*–B*v*) Adenosine reduces, but does not abolish, the probability of observing a large  $\text{Ca}^{2+}$  event, as seen in our trial-by-trial histogram for a single bouton (B*ii*) and for a further five boutons, in which  $\% \Delta F/F$  values are plotted for each experiment (B*iii*). The dashed red line (B*i* and B*ii*) represents the threshold level, as described previously. The probability of observing a large  $\text{Ca}^{2+}$  event is: ACSF  $\theta = 0.139 \pm 0.05$ ; adenosine  $\theta = 0.065 \pm 0.033$  ( $n = 5$ ) (B*iv*). Predictive probability plots (B*v*) show that the probability of observing a large event in the presence of adenosine decreases (red dashed line), whereas the probability of observing a small event increases (solid red line). Both large and small events show a leftward shift in amplitude in adenosine, consistent with adenosine's reported action on  $[\text{Ca}^{2+}]_i$ . (C)  $p_r$  is plotted for each of the six boutons in control conditions and in adenosine using large events as a reporter of  $p_r$ .

Llano, I., Tan, Y.P., and Caputo, C. (1997). Spatial heterogeneity of intracellular  $\text{Ca}^{2+}$  signals in axons of basket cells from rat cerebellar slices. *J. Physiol.* 502, 509–519.

Llano, I., González, J., Caputo, C., Lai, F.A., Blayney, L.M., Tan, Y.P., and Marty, A. (2000). Presynaptic calcium stores underlie large-amplitude miniature IPSCs and spontaneous calcium transients. *Nat. Neurosci.* 3, 1256–1265.

Losonczy, A., Somogyi, P., and Nusser, Z. (2003). Reduction of excitatory postsynaptic responses by persistently active metabotropic glutamate receptors in the hippocampus. *J. Neurophysiol.* 89, 1910–1919.

Mackenzie, P.J., Umeyama, M., and Murphy, T.H. (1996).  $\text{Ca}^{2+}$  imaging of CNS axons in culture indicates reliable coupling between single action potentials and distal functional release sites. *Neuron* 16, 783–795.

Madara, J.C., and Levine, E.S. (2008). Presynaptic and postsynaptic NMDA receptors mediate distinct effects of brain-derived neurotrophic factor on synaptic transmission. *J. Neurophysiol.* 100, 3175–3184.

Malgaroli, A., Ting, A.E., Wendland, B., Bergamaschi, A., Villa, A., Tsien, R.W., and Scheller, R.H. (1995). Presynaptic component of long-term potentiation visualized at individual hippocampal synapses. *Science* 268, 1624–1628.

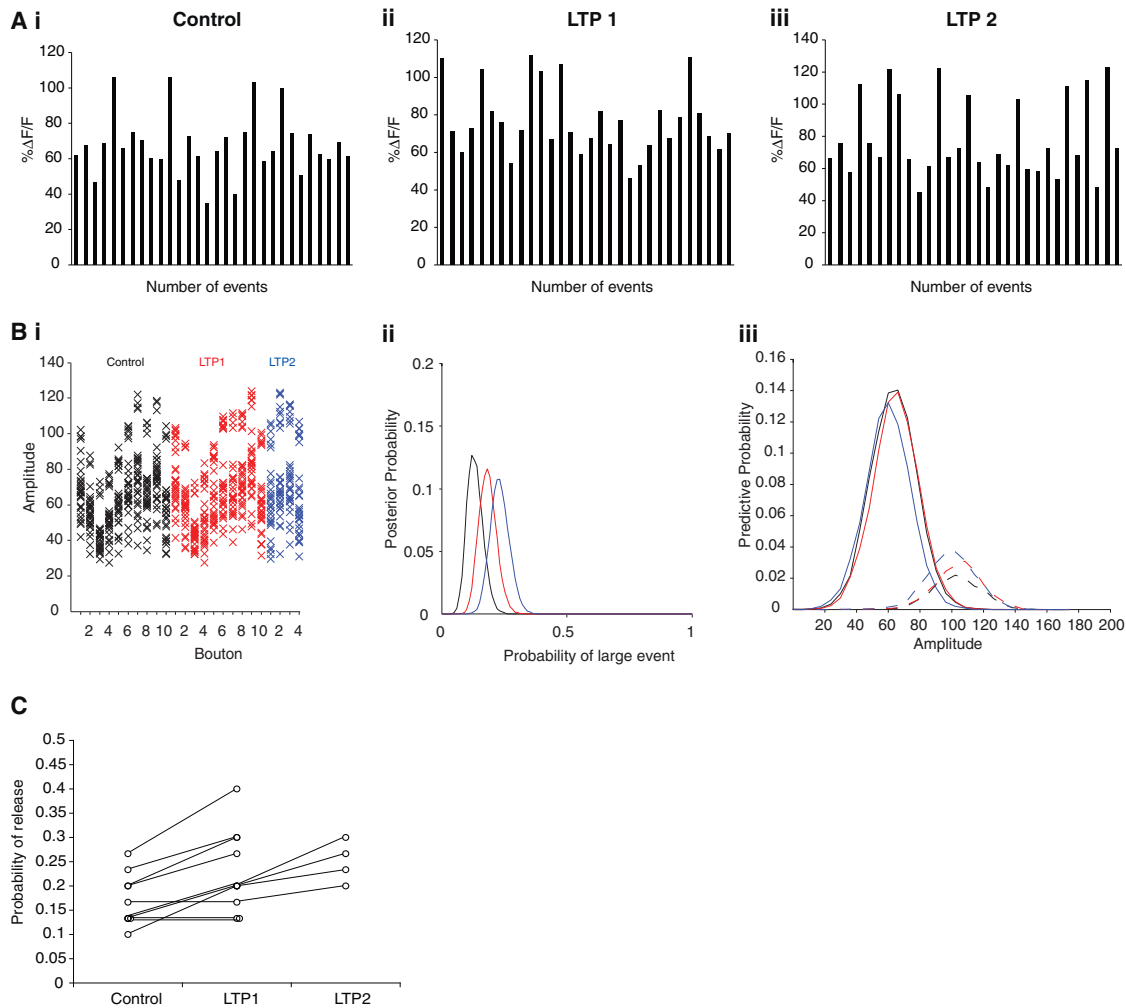


**Figure 12. LTP Increases the Probability of Observing Large  $Ca^{2+}$  Events**

(A i–A iii) LTP, induced using a theta frequency induction protocol, can increase the incidence of large  $Ca^{2+}$  transients in boutons, as seen in the trial-by-trial histograms for a single round (A ii) and for two rounds (A iii) of LTP.

(B i–B iii) In a further nine boutons, in which  $\% \Delta F/F$  values are plotted for each experiment to a single round of LTP (red crosses), the incidence of large  $Ca^{2+}$  is greater for some, but not all, boutons. In contrast, in four boutons, a subsequent round of LTP (blue crosses) increases the incidence of large transients in each case (control  $\theta = 0.134 \pm 0.064$ ; LTP1  $\theta = 0.184 \pm 0.07$ ;  $n = 10$ ; LTP2  $\theta = 0.232 \pm 0.076$ ;  $n = 4$ ) (B i and B ii). Predictive probability plots show that the probability of observing a large event increases (red dashed line), and, after a subsequent round of LTP, increases further (blue dashed line). The amplitude distribution for both small and large events remains unchanged (B iii).

(C)  $p_r$  is plotted for each of the boutons in control conditions and after the induction of LTP1 and LTP2 using large events as a reporter of  $p_r$ .

Mayer, M.L., Westbrook, G.L., and Guthrie, P.B. (1984). Voltage-dependent block by  $Mg^{2+}$  of NMDA responses in spinal cord neurones. *Nature* 309, 261–263.

Meinrenken, C.J., Borst, J.G., and Sakmann, B. (2002). Calcium secretion coupling at calyx of held governed by nonuniform channel-vesicle topography. *J. Neurosci.* 22, 1648–1667.

Mintz, I.M., Sabatini, B.L., and Regehr, W.G. (1995). Calcium control of transmitter release at a cerebellar synapse. *Neuron* 15, 675–688.

Monyer, H., Burnashev, N., Laurie, D.J., Sakmann, B., and Seeburg, P.H. (1994). Developmental and regional expression in the rat brain and functional properties of four NMDA receptors. *Neuron* 12, 529–540.

Mulkey, R.M., and Zucker, R.S. (1991). Action potentials must admit calcium to evoke transmitter release. *Nature* 350, 153–155.

Nakazawa, K., Quirk, M.C., Chitwood, R.A., Watanabe, M., Yeckel, M.F., Sun, L.D., Kato, A., Carr, C.A., Johnston, D., Wilson, M.A., and Tonegawa, S. (2002). Requirement for hippocampal CA3 NMDA receptors in associative memory recall. *Science* 297, 211–218.

Neher, E. (1998). Vesicle pools and  $Ca^{2+}$  microdomains: New tools for understanding their roles in neurotransmitter release. *Neuron* 20, 389–399.

Nowak, L., Bregestovski, P., Ascher, P., Herbet, A., and Prochiantz, A. (1984). Magnesium gates glutamate-activated channels in mouse central neurones. *Nature* 307, 462–465.

Ohno-Shosaku, T., Hashimoto-dani, Y., Ano, M., Takeda, S., Tsubokawa, H., and Kano, M. (2007). Endocannabinoid signalling triggered by NMDA receptor-mediated calcium entry into rat hippocampal neurons. *J. Physiol.* 584, 407–418.

- Peddie, C.J., Davies, H.A., Colyer, F.M., Stewart, M.G., and Rodríguez, J.J. (2008). Dendritic colocalisation of serotonin<sub>1B</sub> receptors and the glutamate NMDA receptor subunit NR1 within the hippocampal dentate gyrus: an ultrastructural study. *J. Chem. Neuroanat.* **36**, 17–26.
- Petralia, R.S., and Wenthold, R.J. (1999). Immunocytochemistry of NMDA receptors. *Methods Mol. Biol.* **128**, 73–92.
- Petralia, R.S., Wang, Y.X., and Wenthold, R.J. (1994). The NMDA receptor subunits NR2A and NR2B show histological and ultrastructural localization patterns similar to those of NR1. *J. Neurosci.* **14**, 6102–6120.
- Qian, J., and Saggau, P. (1999). Modulation of transmitter release by action potential duration at the hippocampal CA3-CA1 synapse. *J. Neurophysiol.* **81**, 288–298.
- Racca, C., Stephenson, F.A., Streit, P., Roberts, J.D., and Somogyi, P. (2000). NMDA receptor content of synapses in stratum radiatum of the hippocampal CA1 area. *J. Neurosci.* **20**, 2512–2522.
- Randall, A., and Tsien, R.W. (1995). Pharmacological dissection of multiple types of Ca<sup>2+</sup> channel currents in rat cerebellar granule neurons. *J. Neurosci.* **15**, 2995–3012.
- Reuter, H. (1996). Diversity and function of presynaptic calcium channels in the brain. *Curr. Opin. Neurobiol.* **6**, 331–337.
- Rodríguez-Moreno, A., and Paulsen, O. (2008). Spike timing-dependent long-term depression requires presynaptic NMDA receptors. *Nat. Neurosci.* **11**, 744–745.
- Rusakov, D.A., Wuerz, A., and Kullmann, D.M. (2004). Heterogeneity and specificity of presynaptic Ca<sup>2+</sup> current modulation by mGluRs at individual hippocampal synapses. *Cereb. Cortex* **14**, 748–758.
- Savtchenko, L.P., and Rusakov, D.A. (2004). Glutamate escape from a tortuous synaptic cleft of the hippocampal mossy fibre synapse. *Neurochem. Int.* **45**, 479–484.
- Schikorski, T., and Stevens, C.F. (2001). Morphological correlates of functionally defined synaptic vesicle populations. *Nat. Neurosci.* **4**, 391–395.
- Schmitz, D., Mellor, J., Breustedt, J., and Nicoll, R.A. (2003). Presynaptic kainate receptors impart an associative property to hippocampal mossy fiber long-term potentiation. *Nat. Neurosci.* **6**, 1058–1063.
- Sheng, M., Cummings, J., Roldan, L.A., Jan, Y.N., and Jan, L.Y. (1994). Changing subunit composition of heteromeric NMDA receptors during development of rat cortex. *Nature* **368**, 144–147.
- Simkus, C.R., and Stricker, C. (2002). The contribution of intracellular calcium stores to mEPSCs recorded in layer II neurones of rat barrel cortex. *J. Physiol.* **545**, 521–535.
- Sjöström, P.J., Turrigiano, G.G., and Nelson, S.B. (2003). Neocortical LTD via coincident activation of presynaptic NMDA and cannabinoid receptors. *Neuron* **39**, 641–654.
- Steinert, J.R., Postlethwaite, M., Jordan, M.D., Chernova, T., Robinson, S.W., and Forsythe, I.D. (2010). NMDAR-mediated EPSCs are maintained and accelerate in time course during maturation of mouse and rat auditory brainstem in vitro. *J. Physiol.* **588**, 447–463.
- Stocca, G., and Vicini, S. (1998). Increased contribution of NR2A subunit to synaptic NMDA receptors in developing rat cortical neurons. *J. Physiol.* **507**, 13–24.
- Stoppini, L., Buchs, P.A., and Muller, D. (1991). A simple method for organotypic cultures of nervous tissue. *J. Neurosci. Methods* **37**, 173–182.
- Stricker, C., and Redman, S. (1994). Statistical models of synaptic transmission evaluated using the expectation-maximization algorithm. *Biophys. J.* **67**, 656–670.
- Takumi, Y., Ramírez-León, V., Laake, P., Rinivik, E., and Ottersen, O.P. (1999). Different modes of expression of AMPA and NMDA receptors in hippocampal synapses. *Nat. Neurosci.* **2**, 618–624.
- Thompson, C.L., Drewery, D.L., Atkins, H.D., Stephenson, F.A., and Chazot, P.L. (2002). Immunohistochemical localization of N-methyl-D-aspartate receptor subunits in the adult murine hippocampal formation: Evidence for a unique role of the NR2D subunit. *Brain Res. Mol. Brain Res.* **102**, 55–61.
- Ventriglia, F., and Di Maio, V. (2000). A Brownian model of glutamate diffusion in excitatory synapses of hippocampus. *Biosystems* **58**, 67–74.
- Verstreken, P., Ly, C.V., Venken, K.J., Koh, T.W., Zhou, Y., and Bellen, H.J. (2005). Synaptic mitochondria are critical for mobilization of reserve pool vesicles at *Drosophila* neuromuscular junctions. *Neuron* **47**, 365–378.
- Ward, B., McGuinness, L., Akerman, C.J., Fine, A., Bliss, T.V., and Emptage, N.J. (2006). State-dependent mechanisms of LTP expression revealed by optical quantal analysis. *Neuron* **52**, 649–661.
- Watanabe, S., Hoffman, D.A., Migliore, M., and Johnston, D. (2002). Dendritic K<sup>+</sup> channels contribute to spike-timing dependent long-term potentiation in hippocampal pyramidal neurons. *Proc. Natl. Acad. Sci. USA* **99**, 8366–8371.
- Woodhall, G., Evans, D.I., Cunningham, M.O., and Jones, R.S. (2001). NR2B-containing NMDA autoreceptors at synapses on entorhinal cortical neurons. *J. Neurophysiol.* **86**, 1644–1651.
- Wu, L.G., and Saggau, P. (1994a). Adenosine inhibits evoked synaptic transmission primarily by reducing presynaptic calcium influx in area CA1 of hippocampus. *Neuron* **12**, 1139–1148.
- Wu, L.G., and Saggau, P. (1994b). Presynaptic calcium is increased during normal synaptic transmission and paired-pulse facilitation, but not in long-term potentiation in area CA1 of hippocampus. *J. Neurosci.* **14**, 645–654.
- Zakharenko, S.S., Zablow, L., and Siegelbaum, S.A. (2001). Visualization of changes in presynaptic function during long-term synaptic plasticity. *Nat. Neurosci.* **4**, 711–717.
- Zakharenko, S.S., Zablow, L., and Siegelbaum, S.A. (2002). Altered presynaptic vesicle release and cycling during mGluR-dependent LTD. *Neuron* **35**, 1099–1110.